Dissolved Nitrogen Cycling in The Eastern Canadian Arctic Archipelago and Baffin Bay from Stable Isotopic Data

Holly C. Westbrook[1], Annie Bourbonnais[1], Cara C M Manning[2], Jean-Eric Tremblay[3], Mohamed Ahmed[4], Brent Gordon Thomas Else[4], and Julie Granger[5]

[1]University of South Carolina
[2]University of British Columbia
[3]Laval University
[4]University of Calgary
[5]University of Connecticut

August 2, 2023

Abstract

Climate change is expected to alter the input of nitrogen (N) sources in the Eastern Canadian Arctic Archipelago (ECAA) and Baffin Bay due to increased discharge from glacial meltwater and permafrost thaw. Since dissolved inorganic N is generally depleted in surface waters, dissolved organic N (DON) could represent a significant N source fueling phytoplankton activity in Arctic ecosystems. Yet, few DON data for this region exist. We measured concentrations and stable isotope ratios (δ15N and δ18O) of DON and nitrate (NO3-) to investigate the sources and cycling of dissolved nitrogen in regional rivers and at the sea surface from samples collected in the ECAA and Baffin Bay during the summer of 2019. The isotopic signatures of NO3- in rivers could be reproduced in a steady state isotopic model by invoking mixing between atmospheric NO3- and nitrified ammonium as well as NO3- assimilation by phytoplankton. DON concentrations were low in most rivers ([?]4.9 μmol L-1), whereas the concentrations (0.54–12 μmol L-1) and δ15N of DON (-0.71–9.6 sea surface were variable among stations, suggesting dynamic cycling and/or distinctive sources. In two regions with high chl-a, DON concentrations were inversely correlated with chlorophyll-an and the d15N of DON, suggesting net DON consumption in localized phytoplankton blooms. We derived an isotope effect of -6.9data helps establish a baseline to assess future change in nutrient regime for this climate sensitive region.

Dissolved Nitrogen Cycling in The Eastern Canadian Arctic Archipelago and Baffin Bay from Stable Isotopic Data

H.C. Westbrook[1], A. Bourbonnais[1,*], C.C.M. Manning[2], J.-É. Tremblay[3], M. M. M. Ahmed[4], B. Else[4], and J. Granger[2]

[1] School of the Earth, Ocean and Environment, University of South Carolina, Columbia, SC, United States

[2] Department of Marine Sciences, University of Connecticut, Groton, Connecticut, United States

[3] Québec-Océan and Takuvik, Département de biologie, Université Laval, Québec, Québec, Canada

[4] Department of Geography, University of Calgary, Calgary, Alberta, Canada

Corresponding author: Annie Bourbonnais (abourbonnais@seoe.sc.edu)

Key Points:

- Nitrate in regional rivers derived proximately from nitrification.
- Dissolved organic nitrogen concentrations in regional rivers were low.
- Dissolved organic nitrogen consumption was observed in the ECAA and Baffin Bay with highest chlorophyll-a.

Abstract

Climate change is expected to alter the input of nitrogen (N) sources in the Eastern Canadian Arctic Archipelago (ECAA) and Baffin Bay due to increased discharge from glacial meltwater and permafrost thaw. Since dissolved inorganic N is generally depleted in surface waters, dissolved organic N (DON) could represent a significant N source fueling phytoplankton activity in Arctic ecosystems. Yet, few DON data for this region exist. We measured concentrations and stable isotope ratios ($\delta^{15}N$ and $\delta^{18}O$) of DON and nitrate (NO_3^-) to investigate the sources and cycling of dissolved nitrogen in regional rivers and at the sea surface from samples collected in the ECAA and Baffin Bay during the summer of 2019. The isotopic signatures of NO_3^- in rivers could be reproduced in a steady state isotopic model by invoking mixing between atmospheric NO_3^- and nitrified ammonium as well as NO_3^- assimilation by phytoplankton. DON concentrations were low in most rivers ($\leq$4.9 μmol L^{-1}), whereas the concentrations (0.54–12 μmol L^{-1}) and $\delta^{15}N$ of DON (−0.71–9.6 ‰) at the sea surface were variable among stations, suggesting dynamic cycling and/or distinctive sources. In two regions with high chl-a, DON concentrations were inversely correlated with chlorophyll-a and the $\delta^{15}N$ of DON, suggesting net DON consumption in localized phytoplankton blooms. We derived an isotope effect of −6.9‰ for DON consumption. Our data helps establish a baseline to assess future change in nutrient regime for this climate sensitive region.

Plain Language Summary

Primary productivity in the Arctic Ocean surface waters is limited by nitrogen supply. We investigated dissolved inorganic and organic nitrogen dynamics in the Eastern Canadian Arctic Archipelago (ECAA) and Baffin Bay surface ocean waters as well as adjacent rivers. We used the isotopic composition (N and O) of both dissolved organic and inorganic nitrogen (DON and DIN, respectively) to explore the sources and transformations of nitrogen. Nitrate in rivers was from both from the atmosphere and from nitrified ammonium. Nitrate was also consumed by phytoplankton. DON concentrations were low in rivers compared to inorganic nitrogen (i.e., nitrate). This observation contrast with previous data collected in the Eurasian and U.S. western coastal Arctic Ocean, where rivers input a high quantity of DON to the coastal ocean. We observed variable DON concentrations and isotopic composition in the ECAA and Baffin Bay surface ocean waters, suggesting different sources and/or a dynamic DON cycling. We additionally found evidence for DON consumption in regions of highest chlorophyll-a. These data are important to better understand how Greenland's melting ice sheet will impact nutrient delivery and primary productivity in the region.

Introduction

Climate change is rapidly altering Arctic ecosystems. As air and seawater temperatures are rising, sea ice volume is decreasing and seasonal river discharge is increasing (Wu et al., 2005; Wassmann et al., 2011; Bintanja & Selten, 2014; Feng et al., 2021). The critical roles played by the Arctic Ocean in controlling the thermohaline circulation and supporting fisheries (Link & Tol, 2009) have stimulated scientific research in the region within the past few decades. While primary productivity is expected to increase for most Arctic shelves, similar changes are not ubiquitous across the entire Arctic (Arrigo et al., 2015; Lewis et al, 2020). For example, decreased nutrient delivery through physical circulation as well as increased stratification due to higher freshwater input may decrease primary productivity overall in the Canada Basin and the Eastern Canadian Arctic Archipelago (ECAA), including Baffin Bay, the Nares Strait, Lancaster

Sound, and Jones Sound (McLaughlin & Carmack, 2010; Lehmann et al., 2019). Nutrients in the surface waters of the ECAA are typically low unless there are localized sources, such as rivers and inputs from glacially-driven upwelling (Tank et al., 2012; Thibodeau et al., 2017; Cape et al., 2019; Bhatia et al., 2022). The availability of nutrients, as well as access to sunlight, are the key factors controlling primary productivity in the western Arctic basins (Tremblay et al., 2015). Nitrogen is ultimately limiting in the western Arctic (Tremblay et al., 2006; Yamamoto-Kawai et al., 2006) and thus sources and sinks of nitrogen need to be constrained to better understand the current N budget as a baseline to assess future changes.

The ECAA is fed predominantly by Pacific generated water from the Canada Basin moving eastward and exiting at Lancaster Sound. Arctic water also enters through Nares Strait, carrying Pacific water and underlying Atlantic-origin water. In Baffin Bay, Arctic water mixes with underlying Atlantic water directly from the North Atlantic via the West Greenland current. Additionally, freshwater is introduced into the ECAA from river and glacial melt as the coastline of the region is peppered with glaciers and has high permafrost coverage. Based on stoichiometric nutrient tracers and nitrate isotope ratios ($\delta^{15}N$), nutrients are dominantly from Pacific-derived water, albeit mixed with Atlantic-derived waters supplying about 25% of the nitrate (NO_3^-) (Lehmann et al., 2022, and references therein).

Dissolved organic nitrogen (DON) typically accounts for the largest pool of dissolved nitrogen in freshwater and marine surface waters (Sipler & Bronk, 2014). Although dominated by refractory species, the labile fraction of DON can be an essential source of N to primary producers, especially in N limited regions (Bronk et al., 2007; Moschonas et al., 2017; Thibodeau et al., 2017; Knapp et al., 2018). DON is composed of a highly refractory pool, and a smaller labile pool, such as amino acids or DNA, which can be utilized on time scales ranging from hours to years. DON can be produced *in situ* in the oceans through mechanisms such as the viral lysing of bacteria or the loss of prey biomass during feeding by microzooplankton (Sipler & Bronk, 2014). Rivers are one of the major DON sources to the ocean due to the presence of terrestrial organic matter. As a result, DON tends to be higher in coastal areas than in the open ocean, although the utilization of DON is not limited to coastal regions. DON can be produced by surface plankton in productive areas and then transported out into N limited regions, fueling primary productivity (Letscher et al., 2013; Knapp et al., 2018; Bif et al., 2022).

The Arctic Ocean is heavily impacted by rivers, receiving 10% of global river discharge despite accounting for only 4% of the global ocean surface (Wu et al., 2005; Holmes et al., 2012). River runoff, permafrost thaw and coastal erosion are significant sources of nutrients in Arctic coastal regions (Tank et al., 2012; Le Fouest., 2013; Treat et al., 2016; Thibodeau et al., 2017; Terhaar et al., 2021). Riverine input is typically high in areas such as the Laptev Sea and the western Arctic which are fed by large rivers. For example, the Lena River and the Mackenzie River have total dissolved nitrogen (TDN) concentrations around 15 to 20 μmol N L^{-1} and discharge into the Laptev Sea and the Beaufort Sea, respectively. Dissolved inorganic N delivered by rivers is immediately consumed, as surface coastal Arctic waters are generally devoid of NO_3^- (Emmerton et al., 2008; Tremblay et al., 2014; Tremblay et al., 2015). The fate of riverine DON in coastal marine waters is still unclear, whether it is utilized, or simply diluted through mixing with DON-deplete waters. For instance, in the Arctic surface ocean, DON concentrations are on average 4.7 μmol N L^{-1}, which is less than the concentrations in major Arctic rivers, which range from 7.4–18.4 μmol N L^{-1} (Sipler & Bronk, 2014). Several studies support that riverine DON in the Arctic is slowly remineralized, representing a significant source

of bioavailable N to the open ocean. Tank et al. (2012) suggested that riverine NO_3^- and DON in the coastal Laptev Sea region contribute to primary productivity, albeit for a relatively small fraction (<10% each) of the overall Arctic Ocean primary production. Thibodeau et al. (2017) found that DON concentrations discharged from the Lena River in the Eurasian Arctic were up to six times higher than riverine NO_3^- concentrations and that DON was rapidly consumed nearshore, with over 50% of it disappearing before reaching the shelf. However, Dittmar et al. (2001) concluded that DON input from Siberian rivers did not substantially support primary productivity, as it was largely recalcitrant. With riverine discharge increasing since around the 1960s (Peterson et al., 2002; Wu et al., 2005), the extent to which rivers influence the delivery of bioavailable DON in Arctic coastal waters needs to be further investigated.

While previous studies have largely focused on the inputs of nutrient from large rivers in past decades (e.g., Tank et al., 2012; Thibodeau et al., 2017), deliveries of NO_3^- and dissolved organic nitrogen (DON) by small rivers and glacially-fed rivers (i.e. marine terminating glaciers and glacial-fed rivers), and their impacts on coastal oceanic primary productivity in the ECAA and Baffin Bay, has not been as thoroughly explored. Inputs of NO_3^- to surface waters was shown to occur by upwelling induced by rising submarine glacial melt discharge in proximity to the Greenland Ice Sheet and Jones Sound (Cape et al., 2019; Bhatia et al., 2021) and glacial melt (Beaton et al., 2017). However, the input of exogenous DON to the surface ocean from glacial melt has not been considered thus far. Upwelling regions generally see elevated DON concentrations following the increase in biological activity due to NO_3^- input from below (Sipler & Bronk, 2014). Since many rivers are of glacial origin in the ECAA and Baffin Bay, both glacial and terrestrial riverine end members must be constrained in order to identify the sources of DON in this rapidly changing region.

The naturally occurring stable N and O isotope ratios of dissolved N species can be exploited to identify N sources and transformations in environmental samples. The nitrogen $^{15}N/^{14}N$ isotope ratios are reported in delta notation (δ) and units of per mil (‰), where the $^{15}N/^{14}N$ and $^{18}O/^{16}O$ references are atmospheric N_2 for N and Vienna Standard Mean Ocean Water (VSMOW) for O.

$$\delta^{15}N = [(^{15}N/^{14}N_{sample}/\ ^{15}N/^{14}N_{air}) - 1] \times 1000$$

$$\delta^{18}O = [(^{18}O/^{16}O_{sample}/\ ^{18}O/^{16}O_{VSMOW}) - 1] \times 1000$$

The $\delta^{15}N$ of NO_3^- and DON is influenced originally by the $\delta^{15}N$ of its source(s) and secondarily by the fractionation imposed during phytoplankton uptake and DON decomposition (see Knapp et al., 2005). The $\delta^{15}N$ of NO_3^- and DON can thus be diagnostic of dominant sources of new N in a system. The DON produced by N_2-fixing organisms as well as newly nitrified NO_3^- from this source are expected to reflect the low $\delta^{15}N$ of newly fixed ammonium (NH_4^+; −2 to 0‰) (Minagawa & Wada, 1986; Carpenter et al., 1997; Knapp et al., 2018) or N from atmospheric deposition with a similarly low $\delta^{15}N$ (Altieri et al., 2016 and references therein). Conversely, the $\delta^{15}N$ DON released by phytoplankton is more elevated, reflecting the $\delta^{15}N$ of the incident inorganic N substrates. The $\delta^{15}N$ of nitrate varies regionally, posting a global ocean average of 5‰, but the $\delta^{15}N$ of Pacific waters of western Arctic basins is distinctly higher at 8‰ (Knapp et al., 2005; Knapp et al., 2018). DON and NO_3^- produced through newly regenerated N, typically NH_4^+, will often have a lower $\delta^{15}N$ compared to ambient substate pools as lighter isotopes are preferentially excreted (Fawcett et al., 2011).

In turn the $\delta^{18}O$ of NO_3^- is distinct among N sources and also sensitive to NO_3^- production and consumption terms. The $\delta^{18}O$ of NO_3^- in atmospheric deposition is exceptionally high (e.g., Hastings et al., 2003). Nitrate produced by the nitrification of ammonium empirically converges on $\delta^{18}O$ of water. (Casciotti et al. 2010; Buchwald et al., 2012). Assimilatory and dissimilatory NO_3^- consumption results in a parallel increase of both $\delta^{18}O$ and $\delta^{15}N$ in a 1:1 ratio (Granger et al., 2004, 2008) in proportion to nitrate consumed. This relationship can be used to determine the influence of processes other than assimilation on the NO_3^- pool.

The goals of this study are to determine, using an isotopic approach, 1) the dominant sources of NO_3^- and DON in the ECAA and Baffin Bay and 2) the transformations affecting these pools. This study focuses on the Nares Strait, Jones Sound, Lancaster Sound, and Baffin Bay, whose coastal regions are more extensively bordered by glaciers compared to other Arctic regions. This region of the Arctic also experiences high permafrost coverage. Nutrient input from other sources, such as terrestrial rivers, are more significant in other Arctic regions such as the Laptev Sea and the western Arctic (Letscher et al., 2012; Thibodeau et al., 2017). The Eastern Baffin Bay is a highly productive area important for fisheries in Greenland. Determining the sources of nutrient inputs to coastal waters is essential to predict the effect of climate change on primary productivity in these economically important regions.

2 Materials and Methods

2.1 Sample Location and Collection

Samples were collected during Leg 2a and 2b of the ArcticNet expedition aboard the CCGS *Amundsen* from July 5th to August 15th of 2019. The expedition took place in the ECAA including Baffin Bay, the Nares Strait, Lancaster Sound, and Jones Sound. Sampling locations and regional circulation patterns are presented in Figure 1. In this region, prevailing currents flow southward through Nares Strait and into Kane Basin, Smith Sound, and finally Baffin Bay. Additionally, in northwestern Baffin Bay, currents flow eastward from Lancaster Sound into Baffin Bay. At the surface, these water masses are Pacific-derived and circulate in the Canadian and Makarov Basins before entering the ECAA through the Nares Strait and Lancaster Sound, respectively. In Baffin Bay, Atlantic water enters along the southwestern coast of Greenland and travels north until it converges with water flowing south from the Smith Sound and circulates southwards on the eastern side of Baffin Island (Lehmann 2019; 2022; Tang et al., 2004). Atlantic water from the Eurasian Basin of the Arctic Ocean can be found at depth in Baffin Bay (Alkire et al., 2010). Ice cover in this region varies by season and along an east-west gradient, with the lowest coverage in the summer and ice persisting much longer on the western side of Baffin Bay in spring (Tang et al., 2004). Some sea ice in Baffin Bay is formed locally, while some is formed in the Nares Strait and transported south. Ice formed in other channels is typically blocked by landfast ice and does not enter Baffin Bay (Tang et al., 2004).

Samples for DON analysis were collected using 12 L Niskin bottles at depths of 100 m and 80 m, and then upwards to the surface in 10 m intervals. Samples at 100 and 80 m were collected in 15 mL centrifuge tubes, and samples taken above 80 m were collected in 60 mL HDPE plastic bottles. All centrifuge tubes and bottles were acid-washed and rinsed three times with sample water prior to collection. All samples were frozen with a headspace to allow for water expansion upon freezing, until analysis. Samples taken during Leg 2b were also filtered with GF/F filters before freezing. Leg 2a samples were filtered prior to analysis with Supor™ 0.45 micron polyethersulfone filters. A comparison was performed on the effect of the different

197 filters on [DON] and $\delta^{15}N$ DON and no significant difference was observed. Riverine samples
198 were collected from surface waters of 11 rivers, filtered with GF/F filters, and frozen. Water
199 samples were also collected for $\delta^{18}O$ of H_2O analysis; samples were collected without bubbles in
200 2 mL glass vials and stored at 4°C.

201 **2.2 Concentration and Isotopic Analysis of DON, NO_3^-, and $\delta^{18}O$ of H_2O**

202 The concentration and $\delta^{15}N$ of DON were measured as in Knapp et al. (2005). Briefly,
203 total dissolved nitrogen (TDN) was oxidized to NO_3^- using recrystallized persulfate followed by
204 measurement on a NO_x analyzer by chemiluminescent detection (Braman & Hendrix, 1989). An
205 unoxidized sample was also used to measure dissolved inorganic nitrogen (DIN). [DON] was
206 estimated as the difference between TDN and DIN. The $\delta^{15}N$ of NO_3^- was then analyzed using
207 the denitrifier method (Sigman & Casciotti, 2001; Weigand et al., 2016).
208 As there is currently no efficient means to remove DIN, the combined concentration and
209 isotopic composition of NO_3^- and NO_2^- (and NH_4^+ if present) must be analyzed to calculate the
210 $\delta^{15}N$ of DON by isotopic mass balance. [NO_3^- + NO_2^-] was thus also measured by
211 chemiluminescence prior to persulfate oxidation and the $\delta^{15}N$ of NO_3^- only (i.e., without the
212 persulfate oxidation step) was determined using the denitrifier method (Sigman & Casciotti,
213 2001; Casciotti et al., 2002; Weigand et al., 2016).
214 [NO_3^-], [NO_2^-] and [PO_4^{3-}] were also measured at sea using a nutrient autoanalyzer.
215 Nitrite concentrations were generally below detection limit in our samples, with maximum
216 values of 1.3 μM in marine samples and 1.4 μM in riverine samples. Only samples in which
217 DON represents over 50% of TDN were considered. Ammonium in riverine samples was
218 measured using a SEAL Nutrient Analyzer.
219 To prepare samples for TDN analysis, 1 mL of freshly prepared persulfate oxidizing
220 reagent (POR) was added to 6 mL of sample in 12 mL threaded test tubes with Teflon-lined
221 phenolic screw caps (Corning 99447-161). These samples were then autoclaved for one hour.
222 POR blank was typically <0.4 μmol N L^{-1} and [TDN] was corrected for blank contribution.
223 Additionally, 5 μmol N L^{-1} of the international standards USGS-40, USGS-64, and USGS-65
224 and an internal standard of 6-aminocaproic acid were analyzed with each run to verify oxidation
225 efficiency and that no fractionation occurred during the persulfate oxidation step. The average
226 percent yield of standard concentrations were >95%, and the standard deviation from known
227 isotopic composition was ±0.37‰.
228 Prior to isotopic analysis, the pH of autoclaved samples, standards, and blanks were
229 adjusted to 3–4 with 6 N HCl. Neutralized samples were injected into 2 mL of *Pseudomonas*
230 *chlororaphis* suspended in media. When analyzing NO_3^- alone, *Pseudomonas aureofaciens* was
231 instead used to measure the $\delta^{18}O$ of NO_3^-. In the few NO_3^- samples in which NO_2^- accumulated,
232 NO_2^- was removed using sulfamic acid as in Granger & Sigman, (2009). The target sample size
233 was 20 nmol. The product N_2O was purified and analyzed using a continuous flow isotope ratio
234 mass spectrometer (Elementar Americas PrecisION) equipped with a custom on-line gas
235 extraction and purge-trap system and PAL autosampler. Samples were standardized using a two-
236 point correction with the international standards IAEA N-3 ($\delta^{15}N$ = 4.7‰ vs air) and USGS-34
237 ($\delta^{15}N$ = −1.8‰ vs air). The $\delta^{15}N$ of DON was determined by isotopic mass balance taking into
238 consideration the concentration and $\delta^{15}N$ of the POR blank as well as sample NO_3^- and TDN.
239 The average standard deviation for duplicate $\delta^{15}N$-DON analysis was generally lower than
240 ±0.5‰. Error propagation was determined using a Monte Carlo method as in Knapp et al.
241 (2018).

The $\delta^{18}O$ of H_2O was measured using an integrated off-axis cavity absorption spectrometer (Los Gatos Research, LGR, Triple Liquid Water Isotope Analyzer, model 912-0032) at the University of Calgary as described in Ahmed et al. (2020). Chlorophyll-a was measured using High Performance Liquid Chromatography (HPLC) at the University of British Columbia as described in Burt et al. (2018). Plots of surface data and cross-sections were generated with the Ocean Data View software (Schlitzer, 2021).

2.3 Mixing Model

$\delta^{18}O$ of H_2O and salinity were used in the following simple mixing model in order to determine the relative contributions of marine water (*mar*), freshwater (*fw*), and sea ice melt (*sim*).

$$f_{mar} + f_{fw} + f_{sim} = 1$$
$$f_{mar} * S_{mar} + f_{fw} * S_{fw} + f_{sim} * S_{sim} = S_{measured}$$
$$f_{mar} * O_{mar} + f_{fw} * O_{fw} + f_{sim} * O_{sim} = O_{measured}$$

Wherein *f* is the fraction of each end member, *S* is salinity and *O* is $\delta^{18}O$ of H_2O. End member values used in the calculations are listed in Table 2.1. There are two important freshwater sources in our system: rivers and glacial water. These two sources have identical salinities (0) and overlapping $\delta^{18}O$ of H_2O values, −17 to −25‰ for river water and −20.5 to −21.7‰ for glacial water (Bedard et al., 1981; Thibodeau et al., 2017; Brown et al., 2020;). Thus we cannot distinguish between these end members with this dataset, and used a value of −20 ‰ for the freshwater $\delta^{18}O$ end member. The contribution of sea ice melt can be considered in two regards: as net sea ice melt or local sea ice melt. Net sea ice melt is integrated over time and reflects the difference between ice formation during the winter and ice melt during the spring and summer. Local sea ice melt is the instantaneous contribution of sea ice melt at the time of sampling. In both cases, a positive value indicates melting, and a negative value indicates formation. Because the melting and formation of sea ice are decoupled in time and space, the contribution of sea ice melt determined from the end members in Table 2.1 represents net sea ice melt rather than local sea ice melt, and local sea ice melt is not determined in this study.

Additionally, because this region has marine water originating from both the Pacific and Atlantic Oceans, we first determine the fraction of Pacific (f_{PW}) and Atlantic water (f_{AW}) in a given sample, assuming that $f_{PW} + f_{AW} = 1$ (Jones et al., 1998; Yamamoto-Kawai et al., 2008; Sherwood et al., 2021; Lehmann et al. 2022). We utilize N^*, a semi conservative nutrient tracer based on the amount of excess DIN relative to phosphate assuming Redfield stoichiometry (i.e., 16N:1P) to determine f_{PW} and f_{AW}. We calculate the N^* of a sample using the equation below, and presume that nitrate is not affected by benthic denitrification in the CAA, a supposition that appears valid (Lehmann et al., 2022).

$$N^* = (NO_3^- - 16 \times [PO_4^{3-}]) + 2.9$$

After N^* was calculated, we calculated f_{PW} in a given sample using the following equation, wherein $N^*_{PW} = -11$ µM, $N^*_{AW} = 2.8$ µM, and negative f_{PW} values indicate no Pacific water contribution and were set to zero.

$$f_{PW} = \frac{N^*_{sample} - N^*_{AW}}{N^*_{PW} - N^*_{AW}}$$

Finally, we adjust our marine endmember mixing model values (S_{mar} and O_{mar}) based on the fraction of Pacific and Atlantic water in the sample. Endmember values for Pacific and Atlantic waters are provided in Table 1.

2.4 Model for Riverine NO_3^- Cycling

A simple steady-state isotopic model was used to apportion the sources and sinks of NO_3^- in ECAA and Baffin Bay rivers. This model included two sources of NO_3^- supplied to rivers: 1) NO_3^- from the nitrification of NH_4^+, which may derive proximately from permafrost, atmospheric NH_4^+, or in-river mineralization (e.g., Wagner et al., 2002; Alves et al., 2013; Fouché et al., 2020) and 2) uncycled NO_3^- from atmospheric deposition (e.g., Hastings et al., 2004). We assumed that complete nitrification of NH_4^+ results in NO_3^- with a $\delta^{15}N$ of ~1.2‰ akin to atmospheric and permafrost end-members (range: −6 to 10‰; (Wynn et al., 2007; Ansari et al., 2013; Louiseize et al., 2014; Heikoop et al., 2015; Arendt et al., 2016; Clark et al., 2020). The $\delta^{18}O$ produced during the nitrification of NH_4^+ was estimated to be ~−14.2 ‰ (range: −8.9 to −19.5‰), assuming that at least 2/3 of the O atoms are derived from water during nitrification (Casciotti et al., 2010; Heikoop et al., 2015; Boshers et al., 2019). For this estimation, we assume the $\delta^{18}O$ of water ranges from −12‰ to −22 ‰ (Wynn et al., 2007; Arendt et al., 2016) and that $\delta^{18}O$ of dissolved oxygen range from 23.7‰ to 24.2‰ based on the $\delta^{18}O$ of air (Horibe et al., 1973; Kiddon et al., 1993; Wang & Veizer, 2000) as in Wynn et al., (2007). Additionally, we assumed isotope effects on the $\delta^{18}O$ NO_3^- and exchange with H_2O during bacterial nitrification as in Casciotti et al. (2010) and Buchwald et al. (2012). We also assumed that NH_4^+ was completely oxidized to NO_3^- in rivers, as NH_4^+ was absent or very low in all our samples, with the highest concentration being 0.56 µM at R-ESC. We assumed that atmospheric deposition added NO_3^- with a $\delta^{15}N$ of −3.5‰ and a $\delta^{18}O$ of 72.1‰ (Hastings et al., 2004; Ansari et al., 2013; Louiseize et al., 2014; Heikoop et al., 2015). We assumed an kinetic N isotope effect (ε) of 5‰ for NO_3^- assimilatiom (Altabet, 2001) and a corresponding $^{18}\varepsilon$:$^{15}\varepsilon$ of 1:1 (Granger et al., 2004). The isotope effect is defined as $^{15}\varepsilon = (({}^{14}k/{}^{15}k) - 1) \times 1000)$, where ^{14}k and ^{15}k are the rate coefficients of the reactions for the light and heavy isotopes respectively. We excluded denitrification, the canonical conversion of NO_3^- to the nitrogen gases N_2O and N_2 under anaerobic conditions, due to the high O_2 concentrations in the rivers (Dalsgaard et al., 2014). We considered two main scenarios for the extent of N recycling and its impact on primary production within the rivers: 1) 50% recycled production, and 2) 25% recycled production. More details about the model are included in the Supporting Information.

We used this model to reproduce the deviation from the $^{18}\varepsilon$:$^{15}\varepsilon$ ratio of ~1 observed for pure NO_3^- assimilation (Granger et al., 2004) of our riverine samples. We refer to this deviation as the Δ(15,18), which is the difference between NO_3^- $\delta^{15}N$ and $\delta^{18}O$ (Rafter et al., 2013).

2.5 Isotope Effect of DON Consumption

In areas where chlorophyll-a was the highest, we estimated the $^{15}\varepsilon$ of DON consumption using a closed system Rayleigh model ($\delta^{15}N$ of DON vs ln([DON])) as in Knapp et al. (2018). A low [DON] concomitant with elevated $\delta^{15}N$ indicates consumption, as kinetic isotope fractionation during consumption increases the $\delta^{15}N$ of the residual DON pool.

3 Results

3.1 Physical Characteristics of the ECAA and Baffin Bay

Near shore waters were influenced by freshwater input from rivers and/or glacial meltwater, as evidenced by fresher surface waters with distinctly low $\delta^{18}O$ H_2O values (−6.05– –0.54‰), suggesting mixing with meteoric water (Mellat et al., 2021). This was evident throughout the study region, more distinct near Talbot Inlet, at the Petermann Glacier, at the Jakobshavn Glacier, in Lancaster Sound, and near the riverine stations R-SG and R-ESC in Jones Sound. (Figure 2). The fraction of freshwater and fraction of sea ice melt in surface waters of the study area are depicted in Figure 2 A&B, respectively. Stations closest to land had a higher fraction of freshwater, as expected. The low fraction of freshwater on the eastern coast of Transect 1 and 2 (0 to 0.05) observed in this study has been attributed to upwelling as well as influence from the West Greenland Current, which is more saline than the Baffin Current (Alkire et al., 2010). Sea ice melt was highest on the western side of Transect 2, which is close to the mouth of the Clyde River.

Many of the rivers sampled in this study were glacially fed, particularly those on Ellesmere Island such as R-ESG and R-6.1. Others were not located near glaciers, for example R-DIW and R-DIW-N on western Devon Island, and R-CP on Cornwallis. River ranged from 0.5 to 3 meters deep and ~1 to ~30 meters wide. $\delta^{18}O$ of H_2O in rivers ranged from −18.4 to −28.4 ‰ (Brown et al., 2022).

3.2 Chlorophyll-a

Chlorophyll-a concentrations at the surface (4 m) were low throughout the study region (typically <2 μg L^{-1}) except in the northern Nares Strait, where a particularly large bloom near Petermann Glacier was observed, as well as in Jones Sound, and the western side of Transect 1 (Figure 3).

3.3 Nitrate Concentration and isotopic composition in the ECAA and Baffin Bay

Nitrate was near zero in all surface waters, except in the Jones sound, as well as the eastern and western ends of the Davis Strait (Transect 1 in Figure 1, Figure 4). At Transect 1 the $\delta^{15}N$ of NO_3^- was lower in the east (6.5‰), and higher in the west (9.8‰),), where higher chlorophyll-a was also observed (Figure 3). $\delta^{18}O$ of NO_3^- across this transect was similar in the east (3.3‰) and west (3.4‰). Additionally at the mouth of Jones sound, a $\delta^{15}N$ and $\delta^{18}O$ of NO_3^- of 14‰ and 50‰ were observed. Nitrate was generally completely consumed in the mixed layer (upper 10 m) within the study area and increased with depth to up to ~15 μM at 100 m depth (Figure S2).

Nitrate concentration and isotopic composition of river samples are provided in Table 2. The concentration of NO_3^- among riverine samples covered a broad range, from 0.44 to 47 μM, (Table 2). Nitrite was <0.2 μM in all samples, both riverine and marine, expect for R-6.1, which had 1.4 μM NO_2^-. High variability was observed even in rivers adjacent to one another, such as R-6.1 and R-ESG. The isotopic composition of NO_3^- was highly variable between rivers, indicating variability in NO_3^- sources and/or transformations among these Arctic rivers. R-SG had the lowest $\delta^{15}N$ of NO_3^- (0.71‰) and a NO_3^- concentration of 2.7 μM. R-ESG had the highest $\delta^{15}N$ of NO_3^- (10.3 ‰) and a NO_3^- concentration of 0.44 μM. The adjacent river R-6.1 had a similarly elevated $\delta^{15}N$ of NO_3^- of 10‰ but much higher NO_3^- concentration of 11 μM. The river at R-6.1 was about 20–30 meters wide. In contrast, R-ESG was a river running through

a crevasse adjacent to Eugenie Glacier and was only ~1 meter wide. R-ESG and R-6.1 were drastically different with respect to their $\delta^{18}O$ of NO_3^-, which was −2.7‰ in R-6.1 and 49‰ in R-ESG.

High variation was also observed between R-ESC and R-SG, both of which are west of Grise Fjord. R-SG was around 5 meters wide and ~0.5 meters deep, while R-ESC was roughly 20 meters wide and 1–2 meters deep. Additionally, R-ESC was more inland than R-SG. R-SG and R-ESC had similar NO_3^- concentrations, but the $\delta^{15}N$ of NO_3^- was almost 2‰ higher at R-ESC than R-SG. Furthermore, the $\delta^{18}O$ of NO_3^- at R-ESC was nearly 4.5 times lower than that at R-SG. Conversely, two other stations in similar areas, R-DIW and R-DIW-N, both located on the west side of Devon Island had significantly different NO_3^- concentrations (20 μM and 47μM, respectively), but similar isotopic signatures (4.4‰ & 4.8‰, respectively).

We consider that the isotopic composition of riverine NO_3^- derived from two end-member sources, namely NO_3^- produced proximately by nitrification and uncycled atmospheric NO_3^-. However, the NO_3^- isotopic composition of our samples did not fall along the mixing line for the two end members. The isotope values were potentially explained by also invoking the partial assimilation of NO_3^- and associated isotopic enrichment of residual NO_3^- (Figure 5). This indicates that atmospheric depositions, assimilation and nitrification contributed, to some extent, to the $\delta^{15}N$ and $\delta^{18}O$ of NO_3^- signatures of the river samples.

Additionally, we used a steady-state isotopic model to confirm that these 3 processes (nitrification, atmospheric depositions and NO_3^- assimilation) could produce the deviation from the $^{18}\varepsilon$:^{15} ε ratio of ~1 observed for pure NO_3^- assimilation (Granger et al., 2004) for our riverine samples. We define the deviation from the $^{8}\varepsilon$:^{15} ε ratio of ~1 as the difference between NO_3^- $\delta^{15}N$ and $\delta^{18}O$, referred to as Δ(15,18) (Rafter et al., 2013). Assuming that 25% of the dissolved nitrogen was recycled within the rivers, we were able to reproduce the full range of observed Δ(15,18) (Figure 6).

3.4 DON Distribution and $\delta^{15}N$ in the ECAA and Baffin Bay

The surface distribution of DON concentrations and the $\delta^{15}N$ of DON are shown in Figure 7. DON concentrations were highly variable but had similar values between regions, ranging from 3.2 to 6.1 μmol N L^{-1} in Baffin Bay and 3.2 to 6.0 μmol N L^{-1} in the Nares Strait. Lancaster Sound and Jones Sound had lower DON concentrations, ranging from 2.1 to 5.7 μmol N L^{-1}. In the mixed layer (upper 10 meters) of the water column, [DON] increased with salinity (Figure 8). This suggests a low [DON] freshwater end member, corroborating our direct riverine measurements of [DON] (mean 1.7 ± 1.5 μM NL^{-1}). [DON] in riverine samples were moderate-to-low (0 – 4.9 μM NL^{-1}), even when NO_3^- was high.

Yet, no significant relationship between [DON] and the fraction of freshwater input was observed in Jones Sound, where the highest freshwater fraction was observed (Figure 2A). [DON] also fell above or below the pure mixing line at other stations, suggesting surface ocean DON production and consumption processes (Figure 8). The relationship between DON concentration and $\delta^{15}N$ with depth was variable and often only characterized within the upper 40 m because NO_3^- concentrations below 40 m depth were often too high to allow calculating the $\delta^{15}N$ of DON from isotopic mass balance. Concentration and $\delta^{15}N$ of DON increased with depth in Transects 1 & 2, Lancaster Sound, and in some areas near Disko Island. DON trends with depth in the Nares Strait were variable. The depth relationship between [DON] and $\delta^{15}N$ was

more variable at some of the more southernmost stations, which either showed an increase in [DON] associated with a slight decrease in $\delta^{15}N$, a slight increase in both $\delta^{15}N$ and [DON] or no change in isotopic composition. The higher [DON] observed for the eastern sections of both transects could have been caused by Ekman-driven upwelling, which is supported by salinity profiles (Figure S1).

In two areas where highest chlorophyll-a concentrations were measured, the Northern Nares Strait and Western Transect 1, chlorophyll-a and DON concentrations in the upper 10 meters were inversely correlated Pearson R^2=0.75 and p-value = 0.04, Spearman $\rho = -1$ and ln([DON]) and $\delta^{15}N$-DON were also inversely correlated (Pearson R^2 = 0.54, p-value = 0.10, Spearman $\rho = -1$ and p-value = 0.02; Figure 10) in these regions. These trends were not observed in Jones Sound, where relatively high chlorophyll-a concentrations were also observed. No relationships were observed between the freshwater fraction and [DON] or freshwater fraction and $\delta^{15}N$ of DON in Northern Nares Strait and Western Transect 1, precluding a significant source of low [DON] and elevated $\delta^{15}N$ DON from rivers at these locations.

4 Discussion

4.1 Deciphering NO_3^- sources in the ECAA and Baffin Bay

Nitrate was close to zero in the surface mixed layer at most stations (<10 m depth), though some surface stations had over 1 μM NO_3^- (Figure 4). While some of the rivers sampled had upwards of 10 μM NO_3^-, these elevated concentrations were not observed in coastal marine waters. These data suggest that NO_3^- from the rivers was rapidly consumed or diluted along the coasts. Previous studies of riverine nutrients in the Arctic have similarly found that riverine NO_3^- delivered into coastal Arctic waters was rapidly consumed nearshore (Emmerton et al., 2008; Tremblay et al., 2014; Tremblay et al., 2015). Riverine nutrient input can increase productivity locally in some near-shore regions, but this only represents a relatively minor fraction of net marine primary productivity in the Arctic (Tremblay et al., 2015). While few blooms were identified through discrete chlorophyll-a sampling, satellite data for July and August 2019 in this region show higher chlorophyll-a nearshore (Figure S4).

The concentration and isotopic composition of riverine NO_3^- were highly variable spatially, indicating variable contributions of end-member sources, and production and consumption terms. We considered two main sources of NO_3^- in rivers: atmospheric deposition or the proximate nitrification of NH_4^+ from either permafrost or atmospheric deposition (and internal recycling). Some rivers with low [NO_3^-] had particularly high $\delta^{18}O$, up to 48‰, suggesting a significant fraction of uncycled atmospheric NO_3^-. The $\delta^{18}O$ of NO_3^- from atmospheric deposition in the summer reflects the $\delta^{18}O$ of the O sources, which are ozone (O_3) and hydroxyl radicals (OH). O_3 has a higher $\delta^{18}O$ (90–122‰; (Krankowsky et al., 1995; Johnston & Thiemens, 1997), while OH usually has $\delta^{18}O < 0$ (Hastings et al., 2004). NO_3^- receives two O atoms from O_3, and one from OH, significantly increasing the $\delta^{18}O$ of NO_3^- from atmospheric deposition (65.2 to 79.6‰; Hastings et al., 2004). Additionally, other rivers had a low $\delta^{18}O$ of NO_3^- (7 out of 11 rivers with $\delta^{18}O$ of $NO_3^- < 0$‰), which portends of nitrification of exogenous and recycled NH_4^+. During nitrification, most of the O atoms originate from water, hence the $\delta^{18}O$ of newly nitrified NO_3^- approaches the O isotopic signature of its H_2O source (Boshers et al., 2019). Since freshwater in high latitude systems has a lower $\delta^{18}O$ of H_2O

(~−22‰; (Louiseize et al., 2014; Arendt et al., 2016), the lower $\delta^{18}O$ of NO_3^- observed in some ECAA river waters could indicate a significant input from nitrification.

To determine the contribution of these end members we used a steady-state isotopic model described in section 2.4 and the supporting information, and were able to reproduce the range of observed $\delta^{15}N$, $\delta^{18}O$ as well as $\Delta(15,18)$ in riverine samples (Figure 6). The NO_3^- isotopic signatures (both $\delta^{15}N$ and $\delta^{18}O$) suggested that mixing between atmospheric NO_3^- and nitrified NH_4^+ alone could not account for the observed $\delta^{15}N$ and $\delta^{18}O$. However, including NO_3^- assimilation helped explain the observed dual NO_3^- isotopic values (solid arrow in Figure 5). This requirement for NO_3^- removal by assimilation is corroborated by previous studies, which have observed the uptake of NO_3^- by phytoplankton in Arctic rivers (Snyder & Bowden, 2014; Beaton et al., 2017). Our isotopic model also suggests that the majority of our data appear to be more influenced by the input of microbially-derived (nitrified) NO_3^- rather than uncycled atmospheric NO_3^-. This indicates that nitrification is putatively an important process to provide bioavailable N to Arctic rivers. Some Canadian Arctic permafrost is known to have a large quantity of NH_4^+ (Fouché et al., 2020), and contact with permafrost can influence the chemical composition of rivers (Frey et al., 2007; Frey & McClelland, 2009; Heikoop et al., 2015; Vonk et al., 2015). Additionally, NH_4^+ can be found in atmospheric deposition in similar proportions to atmospheric NO_3^- (Clark et al., 2020; Fouché et al., 2020). Moreover, NO_3^- input from atmospheric deposition appears to be temporally variable. In the Canadian Arctic, atmospheric deposition can be a dominant source of NO_3^- in rivers during the early melt season, which was from early June to mid−July. Rivers in this study were sampled after this melt season, during which remineralization takes over as the dominant source of NO_3^- (Louiseize et al., 2014). Though nitrification of NH_4^+ derived from permafrost or atmospheric deposition was the predominant source of NO_3^-(or recycling), some rivers had significantly higher NO_3^- concentrations and varying isotopic compositions, even when located geographically in close proximity to one another. For instance, rivers R-6.1 ($[NO_3^-]$ = 11 μM) and R-ESG ($[NO_3^-]$ = 0.44 μM) were adjacent and both had a $\delta^{15}N$ of 10‰, but R-ESG had the lowest $\Delta(15,18)$ (−38‰) and the highest $\delta^{18}O$ of NO_3^- (49‰). In contrast, R-6.1 had a relatively high $\Delta(15,18)$ (13‰), and a lower $\delta^{18}O$ of NO_3^- (−2.7‰). We attribute this extreme variability to different landscape features associated with these rivers. R-ESG was running directly through a glacier, while R-6.1 was next to a glacial moraine containing significant terrestrial material. Therefore, R-ESG was likely in more direct contact with the glacial end member than R-6.1 and thus might have a relatively higher atmospherically-derived NO_3^- fraction. We posit that the sources of nitrogen in these rivers greatly vary depending on watershed characteristics and microbial metabolisms as suggested by Kaiser et al. (2017), even within small spatial scales.

4.2 DON mixing and transformations in the ECAA and Baffin Bay

Several factors control primary productivity in the Arctic, including nitrogen, iron and light availability (Tremblay et al., 2015). Ongoing Arctic sea-ice loss is expected to increase light availability, and drastically impact primary productivity and, consequently biological CO_2 intake (Arrigo, 2007; Frey, 2018; Hill et al., 2018). Furthermore, river discharges from Arctic watersheds are steadily increasing in response to changes in the North Atlantic Oscillation and global mean surface air temperature (Peterson et al., 2002; McClelland et al., 2016; Rood et al., 2017). These rivers transport massive quantities of dissolved and particulate inorganic and organic nitrogen, sustaining primary productivity in coastal waters (Letscher, et al., 2013; McClelland et al., 2016; Thibodeau et al., 2017). Conversely, increased river discharge and

coastal erosion can lead to unfavorable nearshore light conditions, which could negatively impact primary productivity (Terhaar et al., 2021).

In this study, NO_3^- concentrations were extremely low (maximum of 1.3 μM) or zero in the ECAA and Baffin Bay surface waters, which is consistent with N being the limiting nutrient in Arctic regions (Figure 4). However, DON accumulated to concentrations up to 6.1 μmol N L^- in surface waters near Davis Strait (Figure 7A) and could thus sustain primary productivity if a significant fraction of that DON is labile. However, the labile versus recalcitrant DON fractions were not analyzed in this study.

The large differences in both concentrations and isotopic compositions observed in this study could be due to local variations in DON sources. Previous studies have found that the $\delta^{15}N$ of DON can reflect the $\delta^{15}N$ of the new N source (Knapp et al., 2018). Therefore, DON produced from a low $\delta^{15}N$ source, such as newly nitrified NO_3^- from N_2 fixation, can have a similarly low $\delta^{15}N$ DON. In samples where we were able to measure both $\delta^{15}N$ of NO_3^- and DON, the $\delta^{15}N$ of DON was on average ~4 ‰ lower than that of NO_3^- which could indicate DON production from NO_3^-. Knapp et al. (2018) observed a similar trend in the Eastern Tropical South Pacific surface waters, where subsurface DON bracketed the $\delta^{15}N$ of NO_3^- by ±3‰. Additionally, the lack of variation in DON isotopic composition and concentration observed in some areas, such as Transect 4, where [DON] ranged from 5.7–6.1 μmol N L^{-1} and $\delta^{15}N-$ DON ranged from 4.8–4.9‰, could suggest recalcitrant DON (Knapp et al., 2005; Bourbonnais et al., 2009).

Previous studies suggest that rivers are generally a significant source of bioavailable DON. For instance, Lobbes et al. (2000) reported an average [DON] of 12 μM for several Russian rivers. Conversely, Thibodeau et al. (2017) measured DON concentrations ranging between 13.9 to 21.8 μM in the Siberian Arctic. These studies found that up to 70% of the terrigenous DON delivered by Arctic rivers was consumed within the shelf waters of the western and Eurasian Arctic (Letscher et al., 2013; Thibodeau et al., 2017). Our results contrast with findings from other Arctic regions, such as the Siberian and Western Arctic (Lobbes et al., 2000; Dittmar et al., 2001; Holmes et al., 2012; Thibodeau et al., 2017). Rivers measured in this study generally had relatively high NO_3^- but were mostly depleted in DON (up to 4.9 μmol N L^{-1} in R-ESG). Our study thus suggests that rivers in the ECAA and Baffin Bay could act to dilute the DON pool in adjacent coastal marine surface waters. Overall, [DON] seemed to decrease with salinity in the mixed surface layer (upper 10 meters), though this correlation was overall not significant (Figure 8). Increased freshwater inputs with low DON concentrations could further stratify the water column in coastal ECAA and Baffin Bay waters, inhibiting vertical exchange with nutrient-rich deep waters, potentially decreasing primary productivity in the region if DIN is concomitantly low. The differences in DON concentrations observed between studies are likely related to the amount of glacial coverage, as the ECAA and Baffin Bay have significantly higher glacial coverage than the western and Eurasian Arctic (Pfeffer et al., 2014).

DON concentrations reported for glacial rivers are greatly variable. For example, on the Greenland Ice Sheet and the Leverett Glacier, which is adjacent to eastern Transect 1, previous studies reported a range from 5.1–14 μM for DON in the surface ice, while DON in basal ice and summer ice melt was on average about 12 μM and 3.0 μM, respectively (Wadham et al., 2016; Holland et al., 2019). The higher DON values in both locations were attributed to the presence of debris or microbial production of DON. However, other studies reported near zero DON concentration in supraglacial streams, cryoconite melt water, snow, and short ice cores (Telling et al., 2012; Wadham et al., 2016; Holland et al., 2019). In contrast, runoff from the Leverett

Glacier had an average DON concentration of 1.7 μM, with a maximum of 6.3 μM (Wadham et al., 2016). This average value is low relative to the average [DON] of the adjacent marine waters (5.6 μmol N L^{-1}). Thus, the low [DON] seen in river samples in this study could be characteristic of glacial melt that has not significantly mixed with high DON basal ice or debris.

Notably, Western Lancaster Sound, where a particularly high fraction of freshwater was observed, is fed by several rivers which we directly sampled. The rivers R-DIW, R-DIW-N, and R-CP all drain into western Lancaster Sound and had low [DON], ranging from 0.99–2.2 μmol N L^{-1}. This is a lower concentration than the surface ocean [DON] of this region, which is ~4 μmol N L^{-1} but more similar to the [DON] in run off from the Leverett Glacier in the Greenland ice sheet (0.1–6.3 μM, mean of 1.7 μM; Wadham et al., 2016). All the [DON] values of rivers in this study fall within this range, though none of these rivers were draining from the Greenland Ice Sheet. While this can be viewed as a localized input of nutrients, at a larger scale this serves to both stratify and dilute the nearshore nitrogen pool. Thus, our direct measurements of [DON] in Arctic rivers corroborate dilution of the marine DON pool by riverine freshwater. Deviations from a pure mixing line in Figure 8 strongly suggest that competing sources or transformations are affecting the DON pool, e.g., inputs from freshwater and buoyancy or Ekman-driven upwellings and *in-situ* production/consumption by phytoplankton assemblages in the mixed surface waters (Thibodeau et al., 2017; Cape et al., 2019; Bhatia et al., 2022). The DON pool would also be influenced by the lability of the localized sources.

Our isotopic model for riverine NO_3^- suggested that nitrified NH_4^+ was a significant source of NO_3^- in most rivers observed in this study. However, rivers in direct contact with organic matter sources such as permafrost and debris are typically DON-rich (Frey et al., 2007; Frey & McClelland, 2009; Wadham et al., 2016; Fouché et al., 2020). These contrasting observations suggest that most of the NO_3^- in rivers in this study could be atmospherically derived (either from nitrification of NH_4^+ or direct NO_3^- inputs). Future studies should better constrain the isotopic composition ($\delta^{15}N$) and lability of permafrost DON, as well as soil conditions which can affect nitrogen cycling. For example, Frey & McClelland (2007) suggest that organic nitrogen in the permafrost of Alaskan watersheds was more easily remineralized compared to West Siberian watersheds, as the Siberian watersheds have high water saturation, which can limit remineralization of DON and facilitate denitrification. Due to analytical limitations, we were unable to analyze $\delta^{15}N$-DON in all but two of our riverine samples. Improvements to the analytical methods for measuring stable isotopes of DON (e.g., capability to remove DIN prior to DON analysis) could elucidate the contribution of permafrost in delivering DON to glacially fed rivers.

Both R-SG and R-ESG had slightly elevated $\delta^{15}N$-DON (5.8‰ and 7.2‰, respectively). Prior studies have observed low $\delta^{15}N$-DON in rivers and streams, at around −4 to 2‰ (Thibodeau et al., 2017; Ye et al., 2018). These values have been attributed to N sources from atmospheric deposition, aquatic and/or terrestrial N_2 fixation, or plant litter decomposition. Assuming DON sources in these rivers would have similar $\delta^{15}N$ to this range, the values observed here could be considered elevated, and may indicate kinetic isotope fractionation during consumption or a source of recalcitrant DON with a particularly high $\delta^{15}N$. DON consumption will preferentially utilize the lighter isotopes, elevating the $\delta^{15}N$-DON of the remaining pool (e.g., Knapp et al., 2005; Bourbonnais et al., 2009; Knapp et al., 2018). Identifying the sources and lability of DON in these rivers, and the microbial processes involved

could provide further insights on how changes in river discharge and glacial coverage will affect DON supply.

Sea ice melt represents another potential source of DON in the ECAA and Baffin Bay. Similar to surface ice in some glaciers, sea ice can have higher concentration of DON, as observed in the Antarctic (Fripiat et al., 2014; Dall'Osto et al., 2017). Fripiat et al. (2014) suggested high DON was released by microbial communities within the sea ice following NO_3^- assimilation. However, no significant correlation was observed between sea ice melt and DON in this study. Higher resolution sea ice melt and DON datasets, as well as direct measurements of DON in Arctic sea ice could help explore this potential contribution.

4.3 Evidence for DON consumption

DON consumption was identified at two main regions in the study area. One of the signals of DON consumption is isotopic enrichment of the DON pool (Knapp et al., 2018). During consumption, ^{14}N is preferentially taken up, resulting in an increase in the $\delta^{15}N$ of the substrate in surface waters. We observed a negative relationship between chlorophyll-a and DON concentrations in both the northern segment of the Nares Strait and the western half of Transect 1 (Pearson $R^2 = 0.75$, p-value = 0.04, Spearman $\rho = -1$, p-value = 0.02; Figure 9). Though Jones sound also has high chlorophyll, we have excluded it in this analysis as we suspect riverine discharge (Figure S3) is obscuring the relationship between chlorophyll-a, DON, and $\delta^{15}N$ of DON. Additionally, [DON] was negatively correlated with $\delta^{15}N$ (Pearson $R^2 = 0.54$, p-value = 0.10, Spearman $\rho = -1$, p-value = 0.02) (Figure 10). Our derived isotope effect of −6.9‰ using a closed-system Rayleigh model, is comparable to previously measured isotope effects of DON consumption of −5.5‰ (Knapp et al., 2018).

We observe that higher chlorophyll-a is correlated with lower [DON], which contrasts with the relationship found by Knapp et al. (2018). Knapp et al. (2018) observed a positive correlation between surface ocean chlorophyll-a and DON concentrations in the eastern tropical South Pacific, consistent with a photosynthetic source for DON. Conversely, nutrient concentration has been shown to decrease as chlorophyll-a increases due to nutrient uptake by phytoplankton in incubation studies (Cruz et al., 2006; Buapet et al., 2008), and a similar inverse relationship has been observed between DON and chlorophyll-a in lakes (Berman, 1997). We posit that the low DON associated with high chlorophyll-a observed here is the result of net DON uptake by phytoplankton.

Though [DON] remains at around 4–5 μM N L^{-1} in the surface waters throughout most of the study region and NO_3^- is near or at zero, we do not observe a distinct consumption signal at other stations. Several possibilities could explain this observation. First, any correlation between [DON] and chlorophyll-a is likely hindered by the low spatial resolution of available chlorophyll-a measurements, though satellite data corroborates our observations of mostly low chlorophyll-a in Baffin Bay (Figure S4). Second, DON could be recalcitrant in some regions. Dittmar et al. (2001) found that DON in the Siberian Arctic in brackish mixing zones was relatively recalcitrant. Third, DON cycling is likely complex and highly dynamic, with simultaneous consumption and production decoupled in space and time. These processes could complicate the relationship between chlorophyll-a and DON.

5 Conclusions

Nitrogen is a limiting nutrient in the ECAA and Baffin Bay, but its cycling and dynamics are not well constrained, particularly with regards to DON. As river discharges are projected to increase under a warmer climate, it is critical to better understand the role of glacial rivers in delivering nitrogen to this climate sensitive region.

NO_3^- was the dominant dissolved nitrogen species in rivers. Our stable isotopic data suggests that a significant fraction of this NO_3^- was assimilated in the river and/or rapidly consumed near shore. Thus, while increased river discharge may increase riverine NO_3^- flux, the impact on primary productivity may be limited to coastal regions (Tank et al., 2012; Tremblay et al., 2015). We used a steady-state isotopic box model to apportion the sources of NO_3^- in rivers. Our model suggested that NO_3^- assimilation in addition to mixing between inputs from atmospheric deposition and nitrified NH_4^+ is needed to explain the observed $\delta^{15}N$ and $\delta^{18}O$ of NO_3^- in rivers. NO_3^- putatively derived from the nitrification of permafrost or atmospheric NH_4^+ was found to be a main source of NO_3^- in most rivers, while only few rivers (e.g., R-ESG) had significant input of NO_3^- from atmospheric deposition.

DON concentrations were relatively low in rivers (less than 4.9 μmol N L^{-1}). Unlike relationships observed for coastal waters adjacent to major Arctic rivers (Letscher et al., 2013; Tremblay et al., 2014; Thibodeau et al., 2017), we observed that DON concentrations were generally increasing with salinity. We posit that increased riverine discharge in the ECAA and Baffin Bay may result in increased stratification of the surface ocean and dilution of the ambient DON pool, with potential effect on chlorophyll-a. However, it is important to note that geochemical signatures of Arctic rivers can vary seasonally (Alkire et al., 2017; Manning et al., 2020), and our river measurements were collected during a relatively narrow period (July 8th to August 14th, 2019) occurring after the peak annual discharge. Thus, the trends we observed may not be reflective of other times of the year. The low DON concentrations observed in the river contrast with those observed in large terrestrial rivers with extensive watersheds, such as the Mackenzie or Lena Rivers. We observed evidence for DON consumption (i.e., negative correlations between chlorophyll-a and $\delta^{15}N$-DON and DON concentrations) in the northern Nares Strait, as well as western Transect 1. This indicates that DON could be utilized by phytoplnakton in the ECAA and Baffin Bay, although the source of this DON, as well as its composition and lability require further investigation. We estimated an isotope effect for DON consumption of −6.9‰, which is in line with previous studies (−5.5‰; Knapp et al., 2018). This study provides a baseline for DON cycling in the ECAA and Baffin Bay and highlights further areas of research needed to better understand N-cycling in this dynamic region.

Acknowledgments, Samples, and Data

This work was funded by the National Science Foundation (NSF) (award #1927755 to Bourbonnais). Research on the CCGS Amundsen was funded by ArcticNet, a Network of Centres of Excellence Canada and the Amundsen Science program, which is supported through Université Laval by the Canada Foundation for Innovation. Data have been submitted to the NSF Arctic Data Center. Additionally, we thank Dr. Nadine Lehmann for providing the R code used for the Figure 1. Sample collection took place off the shores and within the rivers of Inuit, Inughuit Nunaat, and Kalaallit Nunaat land, and samples were analyzed on Congaree and Tsalaguwetiyi land. We thank the crew of the CCGS Amundsen for making this research

668 possible. We also thank Darcy Perin, Maggie Gaspar, Elise Lumsden, Adrianna Webb, Jaquan
669 High, and Miles Hampton for assistance in sample analysis.

670 **References**

671 Ahmed, M. M. M., Else, B. G. T., Capelle, D., Miller, L. A., & Papakyriakou, T. (2020).
672 Underestimation of surface pCO_2 and air-sea CO_2 fluxes due to freshwater stratification in an
673 Arctic shelf sea, Hudson Bay. *Elementa: Science of the Anthropocene*, *8*(1).
674 https://doi.org/10.1525/elementa.084
675 Alkire, M. B., Falkner, K. K., Boyd, T., & Macdonald, R. W. (2010). Sea ice melt and meteoric
676 water distributions in Nares Strait, Baffin Bay, and the Canadian Arctic Archipelago. *Journal*
677 *of Marine Research*, *68*(6), 767–798. https://doi.org/10.1357/002224010796673867
678 Alkire, M. B., Jacobson, A. D., Lehn, G. O., Macdonald, R. W., & Rossi, M. W. (2017). On the
679 geochemical heterogeneity of rivers draining into the straits and channels of the Canadian
680 Arctic Archipelago. *Journal of Geophysical Research: Biogeosciences*, *122*(10), 2527–2547.
681 https://doi.org/10.1002/2016jg003723
682 Altabet, M. A. (2001). Nitrogen isotopic evidence for micronutrient control of fractional NO_3^-
683 utilization in the equatorial Pacific. *Limnology and Oceanography*, *46*(2), 368–380.
684 Altieri, K. E., Fawcett, S. E., Peters, A. J., Sigman, D. M. & Hastings, M. G. Marine biogenic
685 source of atmospheric organic nitrogen in the subtropical North Atlantic. Proc National Acad
686 Sci 113, 925–930 (2016).
687 Alves, R. J. E., Wanek, W., Zappe, A., Richter, A., Svenning, M. M., Schleper, C., & Urich, T.
688 (2013). Nitrification rates in Arctic soils are associated with functionally distinct populations
689 of ammonia-oxidizing archaea. *The ISME Journal*, *7*(8), 1620–1631.
690 https://doi.org/10.1038/ismej.2013.35
691 Ansari, A. H., Hodson, A. J., Heaton, T. H. E., Kaiser, J., & Marca-Bell, A. (2013). Stable
692 isotopic evidence for nitrification and denitrification in a High Arctic glacial ecosystem.
693 *Biogeochemistry*, *113*(1–3), 341–357. https://doi.org/10.1007/s10533-012-9761-9
694 Arendt, C. A., Heikoop, J. M., Newman, B. D., Wilson, C. J., Graham, D. E., Dafflon, B., et al.
695 (2016). Isotopic and Chemical Identification of Hydrological Pathways in a Watershed
696 Underlain by Shallow Discontinuous Permafrost, *2016*, GC43E–1199.
697 Arrigo, K. (2007). Physical control of primary productivity in Arctic and Antarctic polynyas.
698 *Elsevier Oceanography Series*, *74*, 223–238.
699 Beaton, A. D., Wadham, J. L., Hawkings, J., Bagshaw, E. A., Lamarche-Gagnon, G., Mowlem,
700 M. C., & Tranter, M. (2017). High-Resolution in Situ Measurement of Nitrate in Runoff from
701 the Greenland Ice Sheet. *Environmental Science & Technology*, *51*(21), 12518–12527.
702 https://doi.org/10.1021/acs.est.7b03121
703 Bedard, P., Hillaire-Marcel, C., & Page, P. (1981). ^{18}O modelling of freshwater inputs in Baffin
704 Bay and Canadian Arctic coastal waters. *Nature*, *293*.
705 Berman, T. (1997). Dissolved organic nitrogen utilization by an Aphanizomenon bloom in Lake
706 Kinneret. *Journal of Plankton Research*, *19*(5), 577–586.
707 Bif, M. B. et al. Controls on surface distributions of dissolved organic carbon and nitrogen in the
708 southeast Pacific Ocean. Mar Chem 244, 104136 (2022).
709 Bintanja, R., & Selten, F. M. (2014). Future increases in Arctic precipitation linked to local
710 evaporation and sea-ice retreat. *Nature*, *509*(7501), 479–482.
711 https://doi.org/10.1038/nature13259

712 Bourbonnais, A., Lehmann, M. F., Waniek, J. J., & Schulz-Bull, D. E. (2009). Nitrate isotope
713 anomalies reflect N_2 fixation in the Azores Front region (subtropical NE Atlantic). *Journal of*
714 *Geophysical Research: Oceans (1978–2012)*, *114*(C3). https://doi.org/10.1029/2007jc004617
715 Braman, R. S., & Hendrix, S. A. (1989). Nanogram Nitrite and Nitrate Determination in
716 Environmental and Biological Materials by Vanadium(III) Reduction with
717 Chemiluminescence Detection. *Analytical Chemistry*, *61*, 2715–2718.
718 Brown, K. A. et al. Geochemistry of Small Canadian Arctic Rivers with Diverse Geological and
719 Hydrological Settings. J Geophys Res Biogeosciences 125, (2020).
720 Brown, K. A., Manning, C. C. M., Jones, S. F., Izett, R. W., Capelle, D. W., Else, B. G. T., Eert,
721 J., Tortell, P. D., McLennan, D., Peucker-Ehrenbrink, B., Williams, W. J. (2022): Canadian
722 Arctic Archipelago Rivers Program: Nutrient, Dissolved Organic Carbon, and Water Isotope
723 Data 2016-2019. PANGAEA, https://doi.org/10.1594/PANGAEA.945702, In: Brown, KA et
724 al. (2022): *Canadian Arctic Archipelago Rivers Program: Geochemical Data 2016-2019*.
725 PANGAEA, https://doi.pangaea.de/10.1594/PANGAEA.945995 (dataset in review)
726 Buapet, P., Hiranpan, R., Ritchie, R. J., & Prathep, A. (2008). Effect of nutrient inputs on
727 growth, chlorophyll, and tissue nutrient concentration of Ulva reticulata from a tropical
728 habitat. *ScienceAsia*, *34*(2), 245. https://doi.org/10.2306/scienceasia1513-1874.2008.34.245
729 Burt, W. J., Westberry, T. K., Behrenfeld, M. J., Zeng, C., Izett, R. W., & Tortell, P. D. (2018).
730 Carbon: Chlorophyll Ratios and Net Primary Productivity of Subarctic Pacific Surface Waters
731 Derived From Autonomous Shipboard Sensors. *Global Biogeochemical Cycles*, *32*(2), 267–
732 288. https://doi.org/10.1002/2017gb005783
733 Cape, M. R., Straneo, F., Beaird, N., Bundy, R. M., & Charette, M. A. (2019). Nutrient release to
734 oceans from buoyancy-driven upwelling at Greenland tidewater glaciers. *Nature Geoscience*,
735 *12*(1), 34–39. https://doi.org/10.1038/s41561-018-0268-4
736 Casciotti, K L, Sigman, D. M., Hastings, M. G., Böhlke, J. K., & Hilkert, A. (2002).
737 Measurement of the Oxygen Isotopic Composition of Nitrate in Seawater and Freshwater
738 Using the Denitrifier Method. *Analytical Chemistry*, *74*(19), 4905–4912.
739 https://doi.org/10.1021/ac020113w
740 Casciotti, Karen L., McIlvin, M., & Buchwald, C. (2010). Oxygen isotopic exchange and
741 fractionation during bacterial ammonia oxidation. *Limnology and Oceanography*, *55*(2), 753–
742 762. https://doi.org/10.4319/lo.2010.55.2.0753
743 Clark, S. C., Granger, J., Mastorakis, A., Aguilar-Islas, A., & Hastings, M. G. (2020). An
744 Investigation into the Origin of Nitrate in Arctic Sea Ice. *Global Biogeochemical Cycles*,
745 *34*(2). https://doi.org/10.1029/2019gb006279
746 Cruz, F. L.-D. la, Valenzuela-Espinoza, E., Millán-Núñez, R., Trees, C. C., Santamaría-del-
747 Ángel, E., & Núñez-Cebrero, F. (2006). Nutrient uptake, chlorophyll-a and carbon fixation by
748 Rhodomonas sp. (Cryptophyceae) cultured at different irradiance and nutrient concentrations.
749 *Aquacultural Engineering*, *35*(1), 51–60. https://doi.org/10.1016/j.aquaeng.2005.08.004
750 Dall'Osto, M., Ovadnevaite, J., Paglione, M., Beddows, D. C. S., Ceburnis, D., Cree, C., et al.
751 (2017). Antarctic sea ice region as a source of biogenic organic nitrogen in aerosols. *Scientific*
752 *Reports*, *7*(1), 6047. https://doi.org/10.1038/s41598-017-06188-x
753 Dalsgaard, T., Stewart, F. J., Thamdrup, B., Brabandere, L. D., Revsbech, N. P., Ulloa, O., et al.
754 (2014). Oxygen at Nanomolar Levels Reversibly Suppresses Process Rates and Gene
755 Expression in Anammox and Denitrification in the Oxygen Minimum Zone off Northern
756 Chile. *MBio*, *5*(6), e01966-14. https://doi.org/10.1128/mbio.01966-14

Dittmar, T., Fitznar, H. P., & Kattner, G. (2001). Origin and biogeochemical cycling of organic nitrogen in the eastern Arctic Ocean as evident from D- and L-amino acids. *Geochimica et Cosmochimica Acta*, *65*(22), 4103--4114.

Emmerton, C. A., Lesack, L. F. W., & Vincent, W. F. (2008). Nutrient and organic matter patterns across the Mackenzie River, estuary and shelf during the seasonal recession of sea-ice. *Journal of Marine Systems*, *74*(3–4), 741–755. https://doi.org/10.1016/j.jmarsys.2007.10.001

Fawcett, S. E., Lomas, M. W., Casey, J. R., Ward, B. B., & Sigman, D. M. (2011). Assimilation of upwelled nitrate by small eukaryotes in the Sargasso Sea. *Nature Geoscience*, *4*(10), 717–722. https://doi.org/10.1038/ngeo1265

Feng, D., Gleason, C.J., Lin, P. et al. Recent changes to Arctic river discharge. Nat Commun 12, 6917 (2021)

Fouché, J., Christiansen, C. T., Lafrenière, M. J., Grogan, P., & Lamoureux, S. F. (2020). Canadian permafrost stores large pools of ammonium and optically distinct dissolved organic matter. *Nature Communications*, *11*(1), 4500. https://doi.org/10.1038/s41467-020-18331-w

Frey, K. (2018). Arctic Ocean Primary Productivity: The Response of Marine Algae to Climate Warming and Sea Ice Decline. *Arctic Report Card 2018], Https://Www. Arctic. Noaa. Gov/Report-Card/Report-Card-2018/ArtMID/7878/ArticleID/778/Arctic-Ocean-Primary-Productivity-The-Response-of-Marine-Algae-to-Climate-Warming-and-Sea-Ice-Decline*.

Frey, K. E., & McClelland, J. W. (2009). Impacts of permafrost degradation on arctic river biogeochemistry. *Hydrological Processes*, *23*(1), 169–182. https://doi.org/10.1002/hyp.7196

Frey, K. E., McClelland, J. W., Holmes, R. M., & Smith, L. C. (2007). Impacts of climate warming and permafrost thaw on the riverine transport of nitrogen and phosphorus to the Kara Sea. *Journal of Geophysical Research: Biogeosciences (2005–2012)*, *112*(G4), n/a-n/a. https://doi.org/10.1029/2006jg000369

Fripiat, F., Sigman, D. M., Fawcett, S. E., Rafter, P. A., Weigand, M. A., & Tison, J. -L. (2014). New insights into sea ice nitrogen biogeochemical dynamics from the nitrogen isotopes. *Global Biogeochemical Cycles*, *28*(2), 115–130. https://doi.org/10.1002/2013gb004729

Granger, J., & Sigman, D. M. (2009). Removal of nitrite with sulfamic acid for nitrate N and O isotope analysis with the denitrifier method. *Rapid Communications in Mass Spectrometry*, *23*(23), 3753–3762. https://doi.org/10.1002/rcm.4307

Granger, J., Sigman, D. M., Needoba, J. A., & Harrison, P. J. (2004). Coupled nitrogen and oxygen isotope fractionation of nitrate during assimilation by cultures of marine phytoplankton. *Limnology and Oceanography*, *49*(5), 1763–1773. https://doi.org/10.4319/lo.2004.49.5.1763

Granger, J., Sigman, D. M., Gagnon, J., Tremblay, J., & Mucci, A. (2018). On the Properties of the Arctic Halocline and Deep Water Masses of the Canada Basin from Nitrate Isotope Ratios. *Journal of Geophysical Research: Oceans*, *123*(8), 5443–5458. https://doi.org/10.1029/2018jc014110

Hastings, M. G., Steig, E. J., & Sigman, D. M. (2004). Seasonal variations in N and O isotopes of nitrate in snow at Summit, Greenland: Implications for the study of nitrate in snow and ice cores. *Journal of Geophysical Research: Atmospheres (1984–2012)*, *109*(D20). https://doi.org/10.1029/2004jd004991

Heikoop, J. M., Throckmorton, H. M., Newman, B. D., Perkins, G. B., Iversen, C. M., Chowdhury, T. R., et al. (2015). Isotopic identification of soil and permafrost nitrate sources

in an Arctic tundra ecosystem. *Journal of Geophysical Research: Biogeosciences*, *120*(6), 1000–1017. https://doi.org/10.1002/2014jg002883

Hill, V. J., Light, B., Steele, M., & Zimmerman, R. C. (2018). Light Availability and Phytoplankton Growth Beneath Arctic Sea Ice: Integrating Observations and Modeling. *Journal of Geophysical Research: Oceans*, *123*(5), 3651–3667. https://doi.org/10.1029/2017jc013617

Holland, A. T., Williamson, C. J., Sgouridis, F., Tedstone, A. J., McCutcheon, J., Cook, J. M., et al. (2019). Dissolved organic nutrients dominate melting surface ice of the Dark Zone (Greenland Ice Sheet). *Biogeosciences*, *16*(16), 3283–3296. https://doi.org/10.5194/bg-16-3283-2019

Holmes, R. M., McClelland, J. W., Peterson, B. J., Tank, S. E., Bulygina, E., Eglinton, T. I., et al. (2012). Seasonal and annual fluxes of nutrients and organic matter from large rivers to the Arctic Ocean and surrounding seas. *Estuaries and Coasts*, *35*(2), 369--382.

Johnston, J. C., & Thiemens, M. H. (1997). The isotopic composition of tropospheric ozone in three environments. *Journal of Geophysical Research: Atmospheres*, *102*(D21), 25395–25404. https://doi.org/10.1029/97jd02075

Kaiser, K., Canedo-Oropeza, M., McMahon, R., & Amon, R. M. W. (2017). Origins and transformations of dissolved organic matter in large Arctic rivers. *Scientific Reports*, *7*(1), 13064. https://doi.org/10.1038/s41598-017-12729-1

Kiddon, J., Bender, M. L., Orchardo, J., Caron, D. A., Goldman, J. C., & Dennett, M. (1993). Isotopic fractionation of oxygen by respiring marine organisms. *Global Biogeochemical Cycles*, *7*(3), 679–694.

Knapp, A. N., Sigman, D. M., & Lipschultz, F. (2005). N isotopic composition of dissolved organic nitrogen and nitrate at the Bermuda Atlantic Time-series Study site. *Global Biogeochemical Cycles*, *19*(1).

Knapp, A. N., Casciotti, K. L., & Prokopenko, M. G. (2018). Dissolved Organic Nitrogen Production and Consumption in Eastern Tropical South Pacific Surface Waters. *Global Biogeochemical Cycles*, *32*(5), 769–783. https://doi.org/10.1029/2017gb005875

Knapp, A. N., Sigman, D. M., & Lipschultz, F. (2005). N isotopic composition of dissolved organic nitrogen and nitrate at the Bermuda Atlantic Time-series Study site. *Global Biogeochemical Cycles*, *19*(1). https://doi.org/10.1029/2004gb002320

Krankowsky, D., Bartecki, F., Klees, G. G., Mauersberger, K., Schellenbach, K., & Stehr, J. (1995). Measurement of heavy isotope enrichment in tropospheric ozone. *Geophysical Research Letters*, *22*(13), 1713–1716. https://doi.org/10.1029/95gl01436

Le Fouest, V., Babin, M. & Tremblay, J.-É. The fate of riverine nutrients on Arctic shelves. Biogeosciences 10, 3661–3677 (2013).

Lehmann, N., Kienast, M., Granger, J., Bourbonnais, A., Altabet, M. A., & Tremblay, J. -É. (2019). Remote Western Arctic Nutrients Fuel Remineralization in Deep Baffin Bay. *Global Biogeochemical Cycles*, *33*(6), 649–667. https://doi.org/10.1029/2018gb006134

Lehmann, N., Kienast, M., Granger, J., & Tremblay, J.-É. (2022). Physical and Biogeochemical Influences on Nutrients Through the Canadian Arctic Archipelago: Insights from Nitrate Isotope Ratios. *Journal of Geophysical Research: Oceans*, *n/a*(n/a), e2021JC018179. https://doi.org/10.1029/2021jc018179

Letscher, R. T., Hansell, D. A., Kadko, D., & Bates, N. R. (2013). Dissolved organic nitrogen dynamics in the Arctic Ocean. *Marine Chemistry*, *148*, 1–9. https://doi.org/10.1016/j.marchem.2012.10.002

Letscher, R. T., Hansell, D. A., Carlson, C. A., Lumpkin, R., & Knapp, A. N. (2013). Dissolved organic nitrogen in the global surface ocean: Distribution and fate. *Global Biogeochemical Cycles*, *27*(1), 141–153. https://doi.org/10.1029/2012gb004449

Lewis KM, van Dijken GL, Arrigo KR. Changes in phytoplankton concentration now drive increased Arctic Ocean primary production. Science. 2020 Jul 10;369(6500):198-202. doi: 10.1126/science.aay8380. Epub 2020 Jul 9. PMID: 32647002.

Link, P. M. & Tol, R. S. J. Economic impacts on key Barents Sea fisheries arising from changes in the strength of the Atlantic thermohaline circulation. Global Environ Change 19, 422–433 (2009).

Lobbes, J. M., Fitznar, H. P., & Kattner, G. (2000). Biogeochemical characteristics of dissolved and particulate organic matter in Russian rivers entering the Arctic Ocean. *Geochimica et Cosmochimica Acta*, *26*, 2973–2983.

Louiseize, N. L., Lafrenière, M. J., & Hastings, M. G. (2014). Stable isotopic evidence of enhanced export of microbially derived NO3- following active layer slope disturbance in the Canadian High Arctic. *Biogeochemistry*, *121*(3), 565–580. https://doi.org/10.1007/s10533-014-0023-x

Manning, C. C. M., Preston, V. L., Jones, S. F., Michel, A. P. M., Nicholson, D. P., Duke, P. J., et al. (2020). River Inflow Dominates Methane Emissions in an Arctic Coastal System. *Geophysical Research Letters*, *47*(10). https://doi.org/10.1029/2020gl087669

McClelland, J. W., Holmes, R. M., Peterson, B. J., Raymond, P. A., Striegl, R. G., Zhulidov, A. V., et al. (2016). Particulate organic carbon and nitrogen export from major Arctic rivers. *Global Biogeochemical Cycles*, *30*(5), 629–643. https://doi.org/10.1002/2015gb005351

McLaughlin, F. A., & Carmack, E. C. (2010). Deepening of the nutricline and chlorophyll maximum in the Canada Basin interior, 2003–2009. *Geophysical Research Letters*, *37*(24). https://doi.org/10.1029/2010gl045459

Mellat, M. et al. Hydroclimatic Controls on the Isotopic ($\delta^{18}O$, $\delta^{2}H$, d-excess) Traits of Pan-Arctic Summer Rainfall Events. Frontiers Earth Sci 9, 651731 (2021).

Peterson, B. J., Holmes, R. M., McClelland, J. W., Vörösmarty, C. J., Lammers, R. B., Shiklomanov, A. I., et al. (2002). Increasing River Discharge to the Arctic Ocean. *Science*, *298*(5601), 2171–2173. https://doi.org/10.1126/science.1077445

Pfeffer, W. T., Arendt, A. A., Bliss, A., Bolch, T., Cogley, J. G., Gardner, A. S., et al. (2014). The Randolph Glacier Inventory: a globally complete inventory of glaciers. *Journal of Glaciology*, *60*(221), 537–552. https://doi.org/10.3189/2014jog13j176

Rafter, P. A., DiFiore, P. J., & Sigman, D. M. (2013). Coupled nitrate nitrogen and oxygen isotopes and organic matter remineralization in the Southern and Pacific Oceans. *Journal of Geophysical Research: Oceans*, *118*(10), 4781–4794. https://doi.org/10.1002/jgrc.20316

Rood, S. B., Kaluthota, S., Philipsen, L. J., Rood, N. J., & Zanewich, K. P. (2017). Increasing discharge from the Mackenzie River system to the Arctic Ocean. *Hydrological Processes*, *31*(1), 150–160. https://doi.org/10.1002/hyp.10986

Schlitzer, R. (2021). Ocean Data Viewer. Retrieved from https://odv.awi.de

Sigman, D. M., Casciotti, K. L., Andreani, M., Barford, C., Galanter, M. B. J. K., & Böhlke, J. K. (2001). A bacterial method for the nitrogen isotopic analysis of nitrate in seawater and freshwater. *Analytical chemistry*, *73*(17), 4145-4153.

Sipler, R., & Bronk, D. (2014). Dynamics of Dissolved Organic Nitrogen. In D. A. Hansel & C. A. Carlson (Eds.), *Biogeochemistry of Dissolved Organic Matter* (Second, pp. 127–232). https://doi.org/10.1016/b978-0-12-405940-5.00004-2

Snyder, L., & Bowden, W. B. (2014). Nutrient dynamics in an oligotrophic arctic stream monitored in situ by wet chemistry methods. *Water Resources Research*, *50*(3), 2039–2049. https://doi.org/10.1002/2013wr014317

Tang, C. C. L., Ross, C. K., Yao, T., Petrie, B., DeTracey, B. M., & Dunlap, E. (2004). The circulation, water masses and sea-ice of Baffin Bay. *Progress in Oceanography*, *63*(4), 183–228. https://doi.org/10.1016/j.pocean.2004.09.005

Tank, S. E., Manizza, M., Holmes, R. M., McClelland, J. W., & Peterson, B. J. (2012). The Processing and Impact of Dissolved Riverine Nitrogen in the Arctic Ocean. *Estuaries and Coasts*, *35*(2), 401–415. https://doi.org/10.1007/s12237-011-9417-3

Telling, J., Stibal, M., Anesio, A. M., Tranter, M., Nias, I., Cook, J., et al. (2012). Microbial nitrogen cycling on the Greenland Ice Sheet. *Biogeosciences*, *9*(7), 2431–2442. https://doi.org/10.5194/bg-9-2431-2012

Terhaar, J., Lauerwald, R., Regnier, P. et al. Around one third of current Arctic Ocean primary production sustained by rivers and coastal erosion. Nat Commun 12, 169 (2021). https://doi.org/10.1038/s41467-020-20470-z

Thibodeau, B., Bauch, D., & Voss, M. (2017). Nitrogen dynamic in Eurasian coastal Arctic ecosystem: Insight from nitrogen isotope. *Global Biogeochemical Cycles*, *31*(5), 836–849. https://doi.org/10.1002/2016gb005593

Treat, C. C., Wollheim, W. M., Varner, R. K. & Bowden, W. B. Longer thaw seasons increase nitrogen availability for leaching during fall in tundra soils. Environ Res Lett 11, 064013 (2016).

Tremblay, J.-É., Raimbault, P., Garcia, N., Lansard, B., Babin, M., & Gagnon, J. (2014). Impact of river discharge, upwelling and vertical mixing on the nutrient loading and productivity of the Canadian Beaufort Shelf. *Biogeosciences*, *11*(17), 4853–4868. https://doi.org/10.5194/bg-11-4853-2014

Tremblay, Jean-Éric, Michel, C., Hobson, K. A., Gosselin, M., & Price, N. M. (2006). Bloom dynamics in early opening waters of the Arctic Ocean. *Limnology and Oceanography*, *51*(2), 900–912. https://doi.org/10.4319/lo.2006.51.2.0900

Tremblay, Jean-Éric, Anderson, L. G., Matrai, P., Coupel, P., Bélanger, S., Michel, C., & Reigstad, M. (2015). Global and regional drivers of nutrient supply, primary production and CO2 drawdown in the changing Arctic Ocean. *Progress in Oceanography*, *139*, 171–196. https://doi.org/10.1016/j.pocean.2015.08.009

Vonk, J. E., Tank, S. E., Bowden, W. B., Laurion, I., Vincent, W. F., Alekseychik, P., et al. (2015). Reviews and syntheses: Effects of permafrost thaw on Arctic aquatic ecosystems. *Biogeosciences*, *12*(23), 7129–7167. https://doi.org/10.5194/bg-12-7129-2015

Wadham, J. L., Hawkings, J., Telling, J., Chandler, D., Alcock, J., O'Donnell, E., et al. (2016). Sources, cycling and export of nitrogen on the Greenland Ice Sheet. *Biogeosciences*, *13*(22), 6339–6352. https://doi.org/10.5194/bg-13-6339-2016

Wagner, D., Spieck, E., Bock, E., & Pfeiffer, E.-M. (2002). Microbial Life in Terrestrial Permafrost: Methanogenesis and Nitrification in Gelisols as Potentials for Exobiological Process (p. 143). Berlin, Heidelberg: Springer Berlin Heidelberg. https://doi.org/10.1007/978-3-642-59381-9_10

Wang, X., & Veizer, J. (2000). Respiration–photosynthesis balance of terrestrial aquatic ecosystems, Ottawa area, Canada. *Geochimica et Cosmochimica Acta*, *64*(22), 3775–3786. https://doi.org/10.1016/s0016-7037(00)00477-4

939 Wassmann, P., Duarte, C. M., Agusti, S., & Sejr, M. K. (2011). Footprints of climate change in
940 the Arctic marine ecosystem. *Global Change Biology*, *17*(2), 1235–1249.
941 https://doi.org/10.1111/j.1365-2486.2010.02311.x
942 Weigand, M. A., Foriel, J., Barnett, B., Oleynik, S., & Sigman, D. M. (2016). Updates to
943 instrumentation and protocols for isotopic analysis of nitrate by the denitrifier method. *Rapid*
944 *Communications in Mass Spectrometry*, *30*(12), 1365-1383.).
945 Wu, P., Wood, R., & Stott, P. (2005). Human influence on increasing Arctic river discharges.
946 *Geophysical Research Letters*, *32*(2). https://doi.org/10.1029/2004gl021570
947 Wynn, P. M., Hodson, A. J., Heaton, T. H. E., & Chenery, S. R. (2007). Nitrate production
948 beneath a High Arctic glacier, Svalbard. *Chemical Geology*, *244*(1–2), 88–102.
949 https://doi.org/10.1016/j.chemgeo.2007.06.008
950 Yamamoto-Kawai, M., Carmack, E., & McLaughlin, F. (2006). Nitrogen balance and Arctic
951 throughflow. *Nature*, *443*(7107), 43–43. https://doi.org/10.1038/443043a
952 Ye, F., Guo, W., Wei, G., & Jia, G. (2018). The Sources and Transformations of Dissolved
953 Organic Matter in the Pearl River Estuary, China, as Revealed by Stable Isotopes. *Journal of*
954 *Geophysical Research: Oceans*, *123*(9), 6893–6908. https://doi.org/10.1029/2018jc014004
955

956 **Tables**

957 **Table 1.** End member values used in the mixing model (from Yamamoto− Kawai et al., 2008
958 and Alkire et al., 2010).

End Member	Salinity (PSU)	$\delta^{18}O$-H_2O (‰)
Pacific Water	33	−0.80
Atlantic Water	35	0.20
Freshwater (rivers & glaciers)	0.0	−20
Sea Ice	4.0	0.05

959

960 **Table 2.** Concentration and $\delta^{15}N$ and $\delta^{18}O$ of NO_3^- and DON, as well as $\Delta(15,18)$ of NO_3^- in
961 river samples (calculated as in Rafter et al., 2013). "R" denotes rivers sampled. Rivers were
962 named based on proximity to geographic features or CTD stations, and are named as follows:
963 Devon Island West (R-DIW), Devon Island East (R-DIE), Copland Point (R-CP), Devon Island
964 West North (R-RIWN), Sydkap Glacier (R-SG), Eastern Sydkap Icecap (R-ESC), Station 6.1 (R-
965 6.1), Eugenie's Sister Glacier (R-ESG), Station 135 (R-135), Ellesmere Island East (R-EE), and
966 Hans Island (R-HI).
967

STATION	**$[NO_3^-]$**	**$\delta^{15}N-NO_3^-$**	**$\delta^{18}O-NO_3^-$**	**$\Delta(15,18)$**	**[DON]**	**$\delta^{15}N-DON$**
R-DIW	20	4.4	−9.3	14	1.6	
R-DIE	1.3	3.4	18	−14	0.54	
R-CP	4.1	2.9	−7.5	10	2.2	
R-DIW-N	47	4.8	−9.6	14	0.99	
R-SG	2.7	0.71	−1.4	2.1	3.1	5.8
R-ESC	3.3	2.6	−6.3	8.9	1.8	
R-6.1	11	10	−2.7	13	0.0	
R-ESG	0.44	10	49	−38	4.9	7.2
R-135	3.5	6.6	7.3	−0.68	0.16	
R-EE	2.7	4.8	10	−5.4	1.5	
R-HI	4.7	5.3	−0.80	6.1	1.4	

968
969
970
971
972
973
974
975
976
977
978
979
980
981

Figures

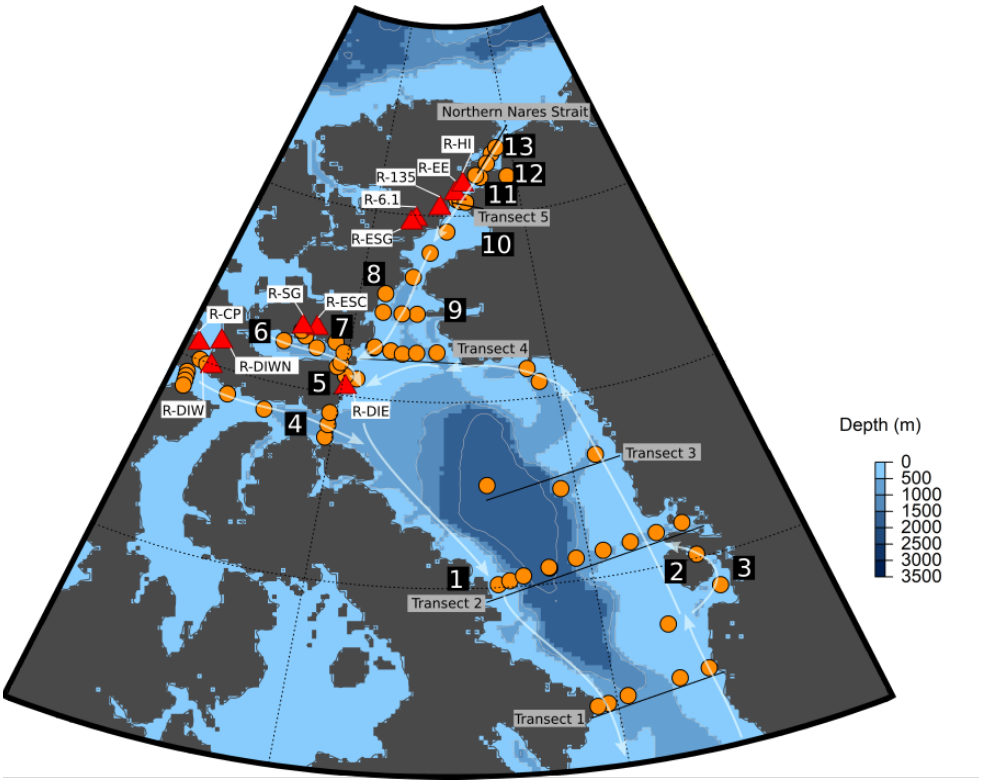

Figure 1. Map of the sampling locations. CTD casts are marked with orange circles. Red triangles represent river locations, which are also labeled by name. Transects 1, 2, 3, 4, 5, and the Northern Nares Strait are also labeled with solid black lines. The directions of surface currents are shown by the white arrows. Important regions and features numbered as follows: 1: Clyde River, 2: Disko Island, 3: Jakobshavn Glacier, 4: Lancaster Sound, 5: Devon Island, 6: Jones Sound, 7: Manson Icefield, 8: Talbot Inlet, 9: Smith Sound, 10: Kane Basin, 11: Kennedy Channel, 12: Petermann Glacier, 13: Hall Basin. 9–13 are all considered part of Nares Strait.

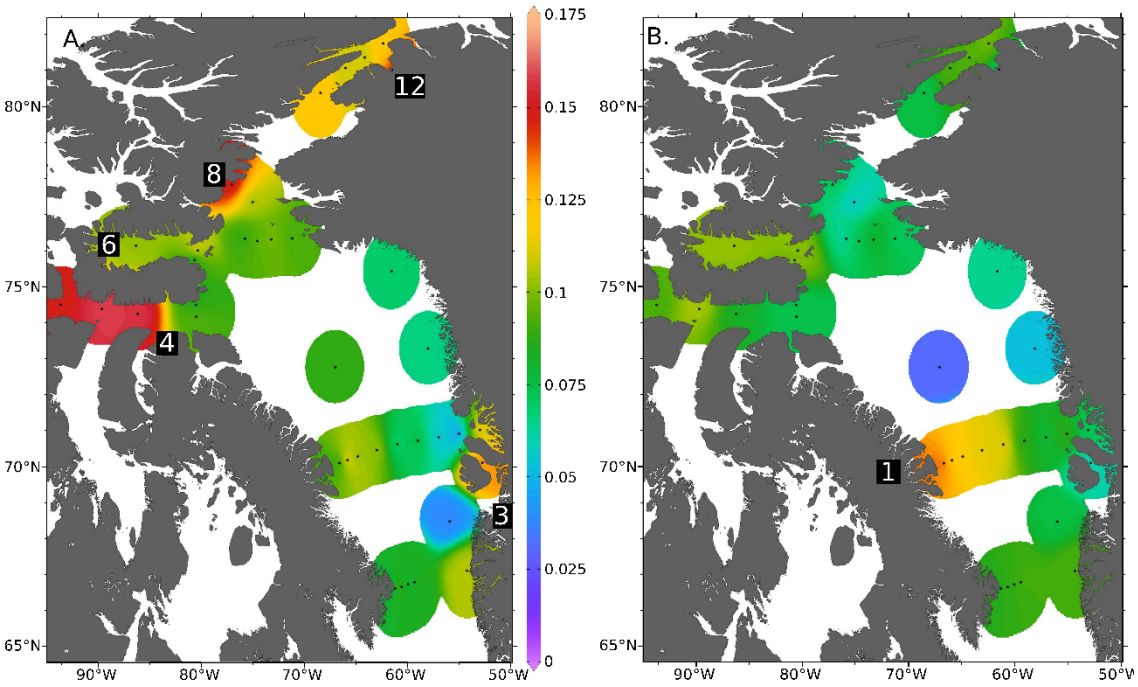

Figure 2. A. Fraction of freshwater and B. fraction of sea ice melt in surface water. 1- Clyde River, 3 – Jakobshavn Glacier, 4 – Lancaster Sound, 6 – Jones Sound, 8 – Talbot Inlet, 12 – Petermann Glacier.

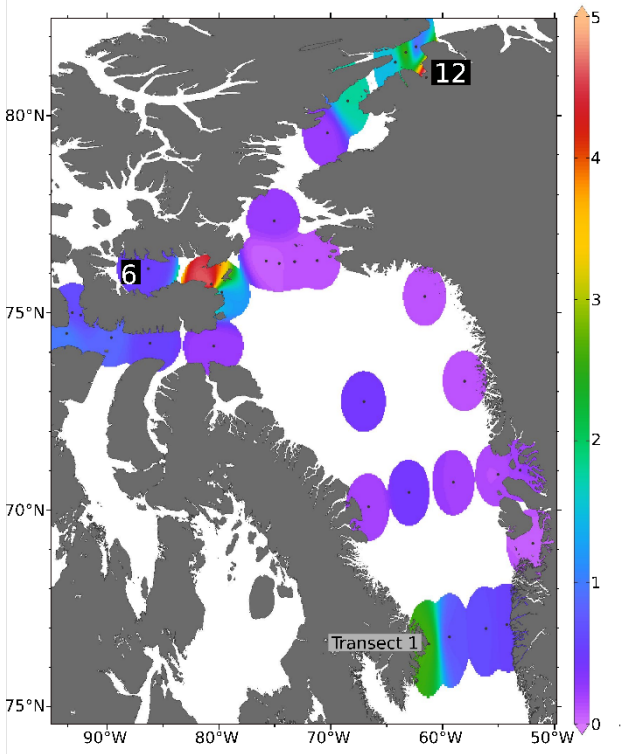

Figure 3. Surface chlorophyll-a (μgL^{-1}), regions with blooms at Petermann Glacier (12), Jones Sound (6), and Western Transect 1

1035

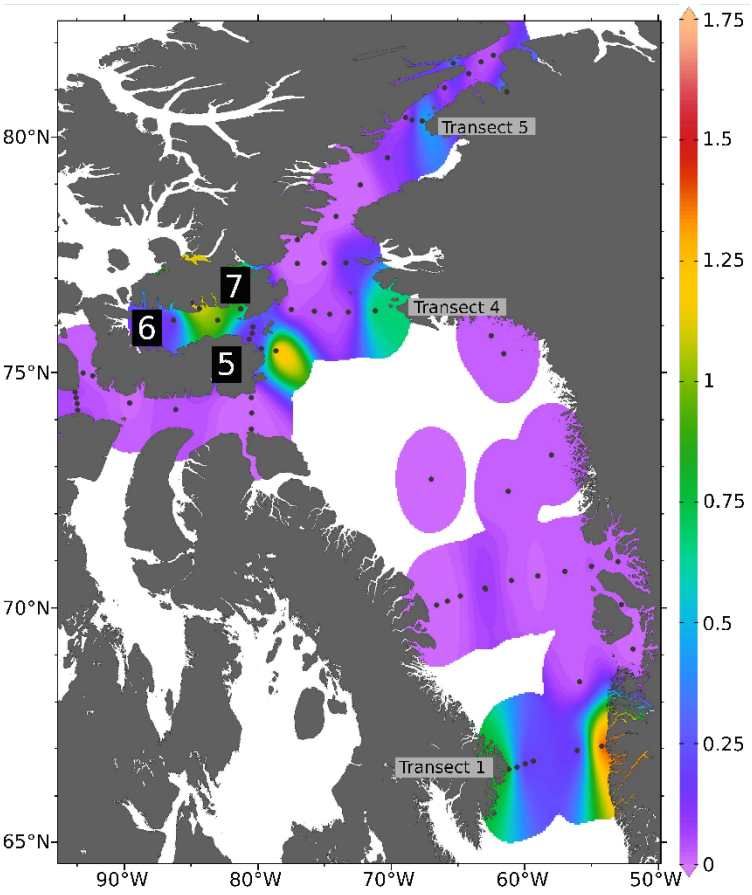

Figure 4. NO_3^- (μM) distribution in the surface of the study area. Regions with measurable NO_3^- concentrations are labeled as in Figure 1.

1057

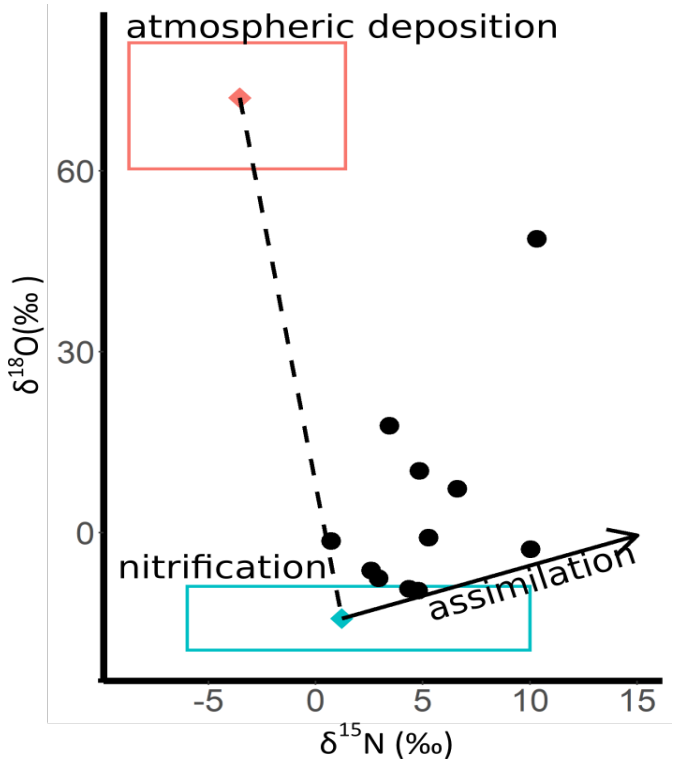

Figure 5. $\delta^{18}O$ vs $\delta^{15}N$ of NO_3^- for riverine samples, with mixing between nitrification of NH_4^+ (blue box) and atmospheric deposition (pink box) marked by the dashed line. The ε^{18}: ε^{15} of assimilation (~1) is noted with the solid black arrow.

1058
1059
1060

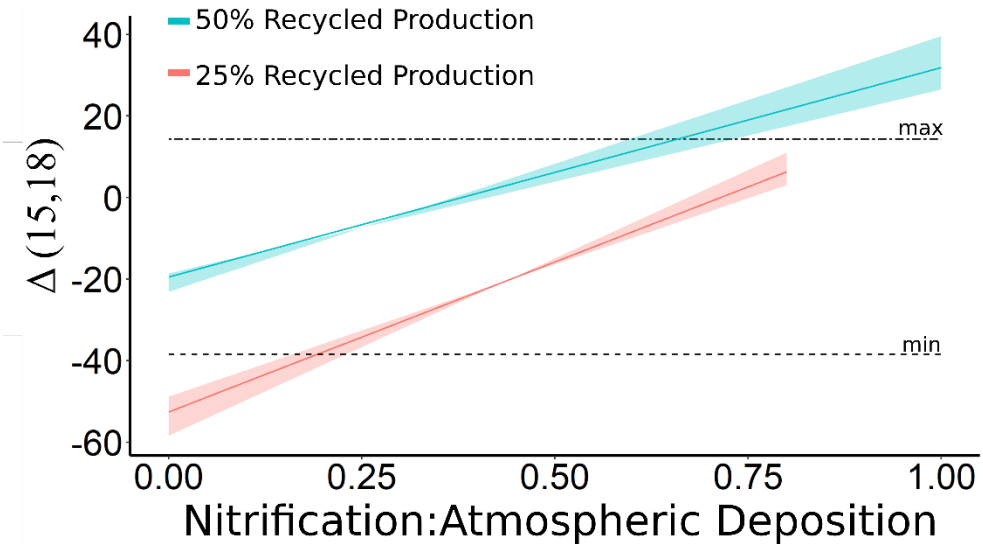

Figure 6. Results from simple box model simulations evaluating the capacity of different sources of NO_3^- in glacial rivers of the ECAA to generate d^{15} Nand d^{18}O and D(15,18) signatures. The ratio of nitrified NH_4^+: atmospheric deposition is on the x axis, and Δ(15-18) on the y-axis. The blue line represents 50% recycled production, and the pink line represents 25% recycled production. The shaded colors represent model outputs when using the outer ranges of the end members. The black dashed lines represent the minimum and maximum Δ(15,18) observed in riverine samples.

1061
1062

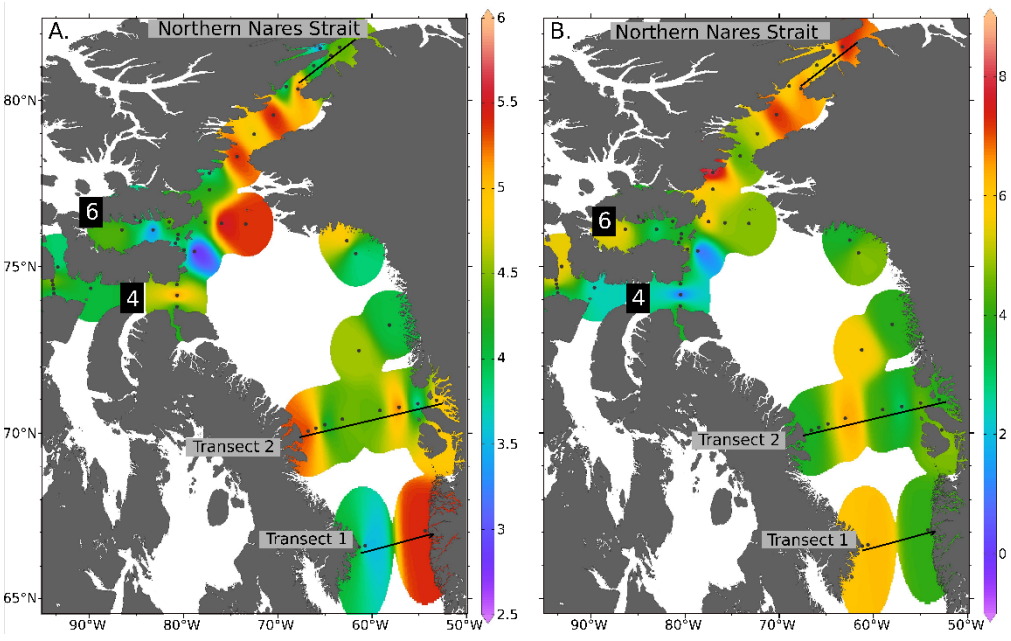

Figure 7. A. [DON] (μM N L^{-1}) and B. δ^{15}N of DON in the surface water. Transects 1, 2, and Northern Nares Strait are denoted with black text. Lancaster (4) and Jones (6) Sounds are also labeled.

1063

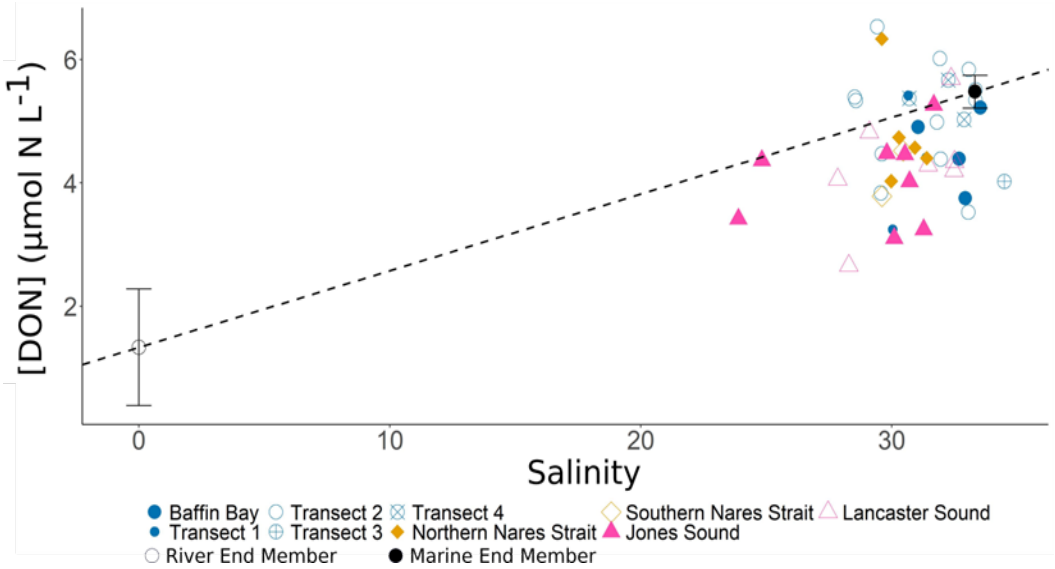

Figure 8. [DON] (µM N L^{-1}) in the mixed layer (upper 10 meters) of the water column vs salinity. Color indicates close geographic proximity: Blue dots represent samples located within Baffin Bay, orange diamonds represent samples in Nares Strait, and pink triangles represent samples located in sounds to the east of Baffin Bay. Riverine (hollow) and marine (solid) end members are marked with black dots with solid lines representing standard deviation in our estimates. The dashed line represents mixing between the two end members. Standard deviation < 0.5 µM for [DON].

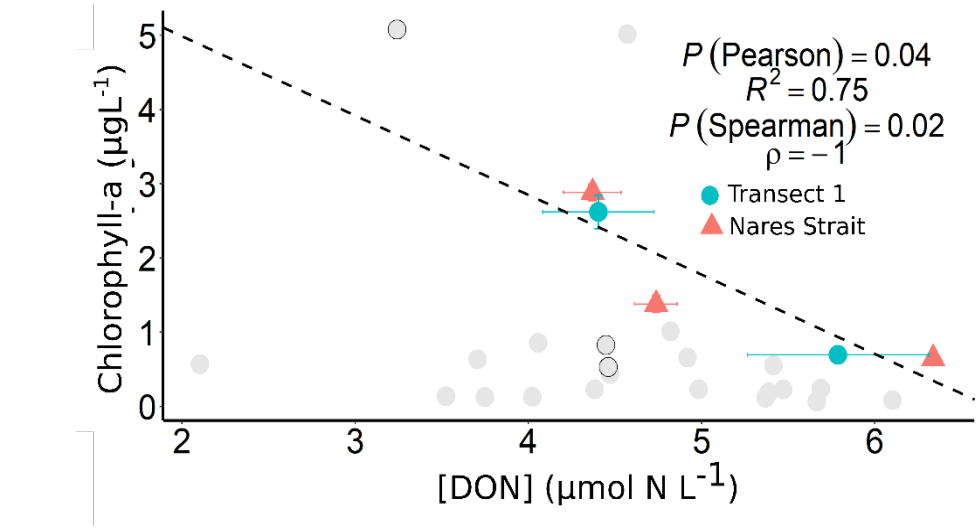

Figure 9. Surface [DON] (µM N L^{-1}) in the northern Nares Strait (north of 80°N) (comprising Hall Basin and Kennedy Channel) and western Transect 1, against chlorophyll-a concentration (µg L^{-1}). The Pearson and Spearman's rank correlation coefficients and p-values (P) are shown. Data from all other stations are shown with light grey dots, with Jones sound outlined in black.

1064
1065

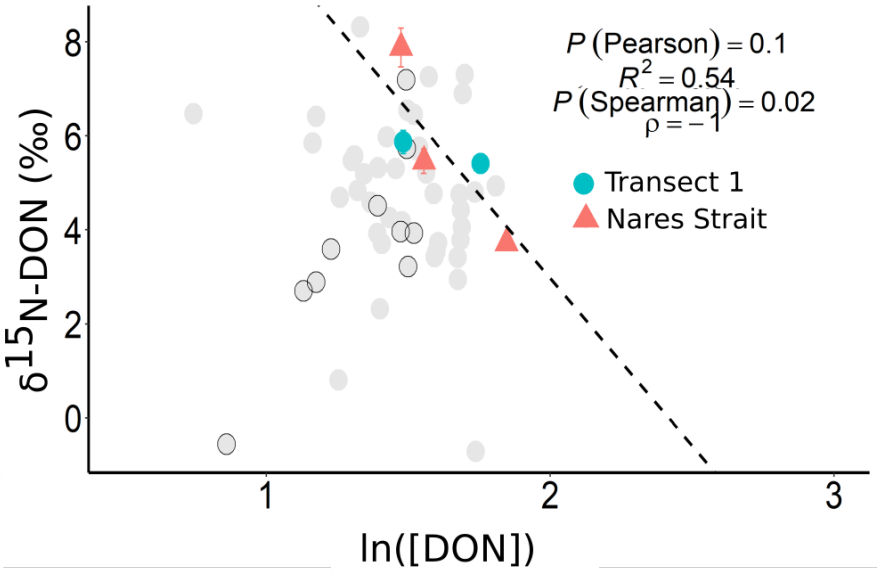

Figure 10. Surface ln(DON) vs $\delta^{15}N$ of DON in the northern Nares Strait (north of 80°N) and western Transect 1. The Pearson and Spearman's rank correlation coefficients and p-values (P) are shown. Data from all other stations are shown with light grey dots, with Jones Sound outlined in black

1066
1067
1068

Global Biogeochemical Cycles

Supporting Information for

Dissolved Nitrogen Cycling in The Eastern Canadian Arctic Archipelago from Stable Isotopic Data

H.C. Westbrook[1], A. Bourbonnais[1], C.C.M. Manning[2], M. Ahmed[3], B. Else[3], R. Izett[4], and J. Granger[2]

[1] School of the Earth, Ocean and Environment, University of South Carolina, Columbia, SC, United States; [2] Department of Marine Sciences, University of Connecticut, Groton, Connecticut, United States; [3] Department of Geography, University of Calgary, Calgary, Alberta, Canada; [4] Department of Oceanography, Dalhousie University, Halifax, Nova Scotia, Canada

Contents of this file

Introduction

The following is a description of the parameters used in our simple steady-state isotopic model for NO_3^- cycling in rivers in the study area. This model is used to qualitatively evaluate if the observed Δ(15-18) of NO_3^- can be reproduced by considering different dissolved NO_3^- sources (nitrification and atmospheric depositions) in glacial rivers. Subsequently, we provide figures of surface salinity and $\delta^{18}O$ of water in the study area, and nitrate depth profiles. Description of River Isotopic NO_3^- model.

Definition of terms

a = nitrified NO_3^- (from permafrost or atmospheric NH_4^+)
b = atmospheric NO_3^- (from glacial snow melt)
d = assimilation of NO_3^-
e = recycled production of NO_3^-
$\delta^{15}N_{nit}$ = $\delta^{15}N$ of NO_3^- produced during complete nitrification of permafrost or atmospherically derived ammonium, average of 1.22‰ (range: -6 to 10‰; Arendt et al. 2016; Heikoop et al. 2016)
$\delta^{18}O_{nit}$= $\delta^{18}O$ of NO_3^- produced though nitrification of ammonium, average of -14.21‰ (range: -19.51 to -8.9‰; assuming $\delta^{18}O$ DO of 23.5-24.2‰ (Kiddon et al., 1993; Wang & Veizer, 2000; Horibe et al., 1973 as in Wynn et al., 2007) and $\delta^{18}O$ H_2O of -12 to -22‰ (Arendt et al. 2016, Wynn et al., 2007))
$\delta^{15}N_{atm}$ = $\delta^{15}N$ of NO_3^- from atmospheric deposition, -3.54‰ (-8.72-1.40; Ansari et al., 2013; Hastings et al., 2003; Heikoop et al., 2015; Louiseize et al., 2014)
$\delta^{18}O_{atm}$ = $\delta^{18}O$ of NO_3^- from atmospheric deposition, 72.07‰ (60.30-80.20; Ansari et al., 2013; Hastings et al., 2003; Heikoop et al., 2015; Louiseize et al., 2014)
ε_{as}^{15} = isotope effect of NO_3^- assimilation on N (5‰; Altabet, 2001)

ε_{as}^{18} = isotope effect of NO_3^- assimilation on O (5.9‰; Rafter & Sigman, 2015)
$\delta^{15}N_{re}$ = $\delta^{15}N$ of NO_3^- from recycled production
$\delta^{18}O_{re}$ = $\delta^{18}O$ of NO_3^- from recycled production average of -14.21‰ (range: -19.51 to -8.9‰; assuming $\delta^{18}O$ DO of 23.5 to 24.2‰ (Kiddon et al., 1993; Wang & Veizer, 2000; Horibe et al., 1973 as in Wynn et al., 2007) and $\delta^{18}O$ H_2O of -12 to -22‰ (Arendt et al. 2016, Wynn et al., 2007))
$\delta^{15}N_{as}$ = $\delta^{15}N_{box}$ - ε_{as}^{15} = $\delta^{15}N$ of NO_3^- assimilated
$\delta^{15}N_{box}$ = model output of $\delta^{15}N$ of NO_3^- in the river

Model Conditions

- Nitrified NO_3^- is a source
- Atmospheric NO_3^- is a source
- NO_3^- assimilation is a sink
- Recycled production accounts for 50% or 25% of supplied NO_3^-
- No denitrification

For $\delta^{15}N$

$$\delta^{15}N_{box} = a \times \delta^{15}N_{nit} + b \times \delta^{15}N_{atm} - [(d - e) \times (\delta^{15}N_{box} - \varepsilon_{as}^{15})]$$

This can be arranged to

$$\delta^{15}N_{box} = \frac{a \times \delta^{15}N_{nit} + b \times \delta^{15}N_{atm} + [(d - e) \times \varepsilon_{as}^{15}]}{(1 + d - e)}$$

For $\delta^{18}O$

$$\delta^{18}O_{box} = a \times \delta^{18}O_{nit} + b \times \delta^{18}O_{atm} - [d \times (\delta^{18}O_{box} - \varepsilon_{as}^{18})] + e \times \delta^{18}O_{re}$$

This can be arranged to

$$\delta^{18}O_{box} = \frac{a \times \delta^{18}O_{nit} + b \times \delta^{18}O_{atm} + d \times \varepsilon_{as}^{18} + e \times \delta^{18}O_{re}}{(1 + d)}$$

The $\Delta(15,18)$ is calculated according to Rafter and Sigman (2016):

$$\Delta(15,18) = \delta^{15}N - \delta^{18}O$$

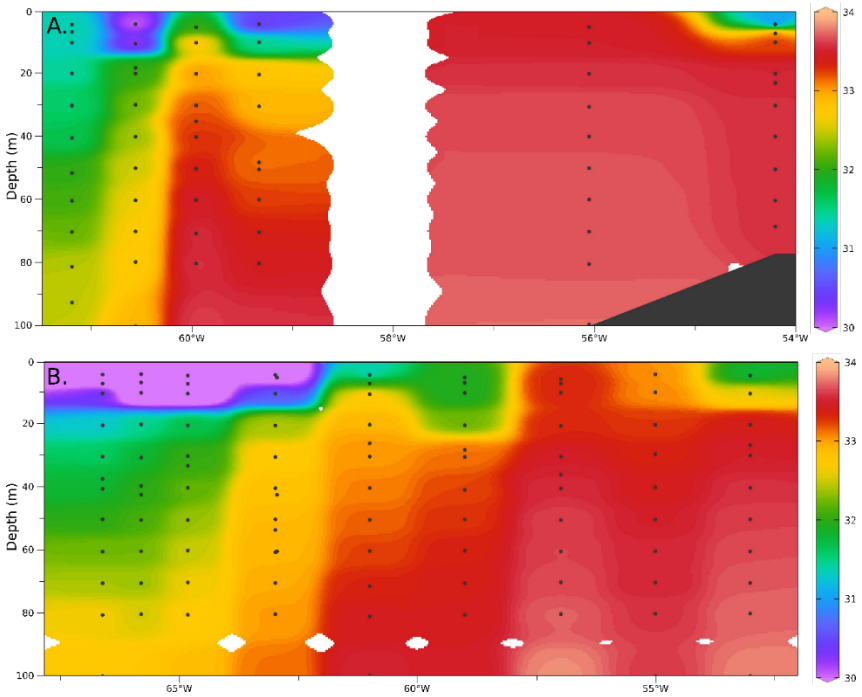

Figure S1: Salinity cross sections of A. Transect 1 and B. Transect 2

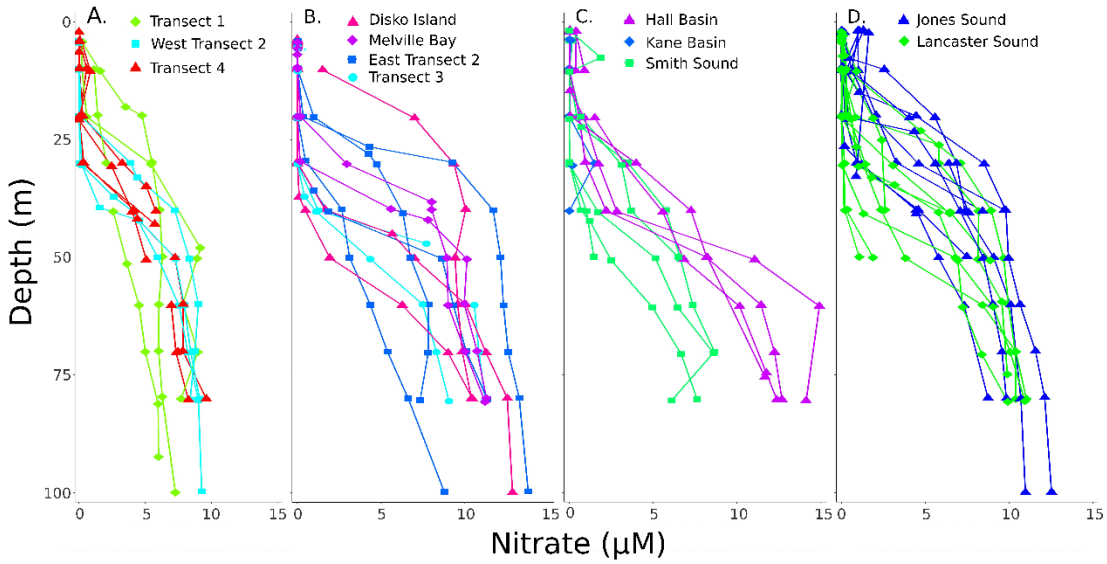

Figure S2: Nitrate depth profiles for A. Western Baffin Bay B. Eastern Baffin Bay C. Nares Strait and D. Jones and Lancaster Sounds

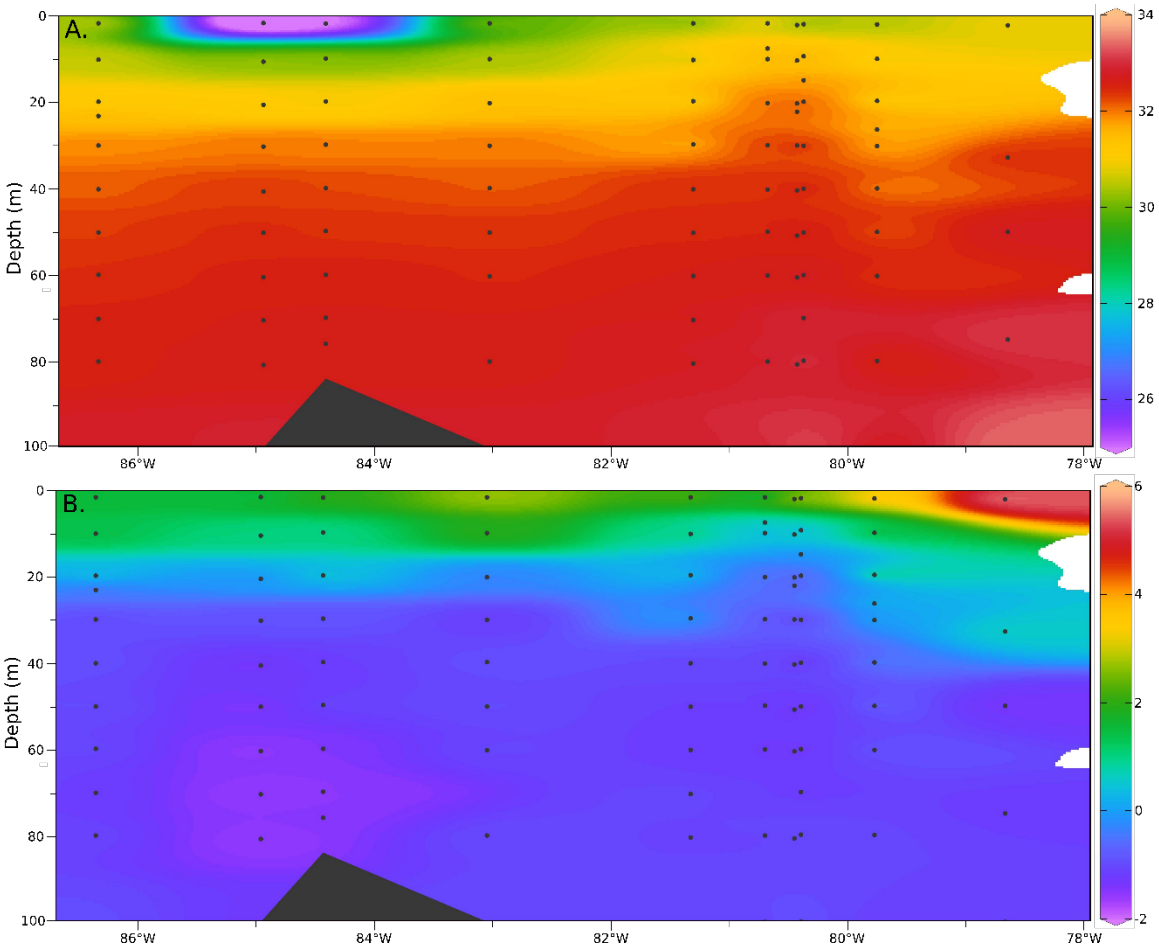

Figure S3: Jones Sound Salinity (A) and Temperature (B) Cross Section.

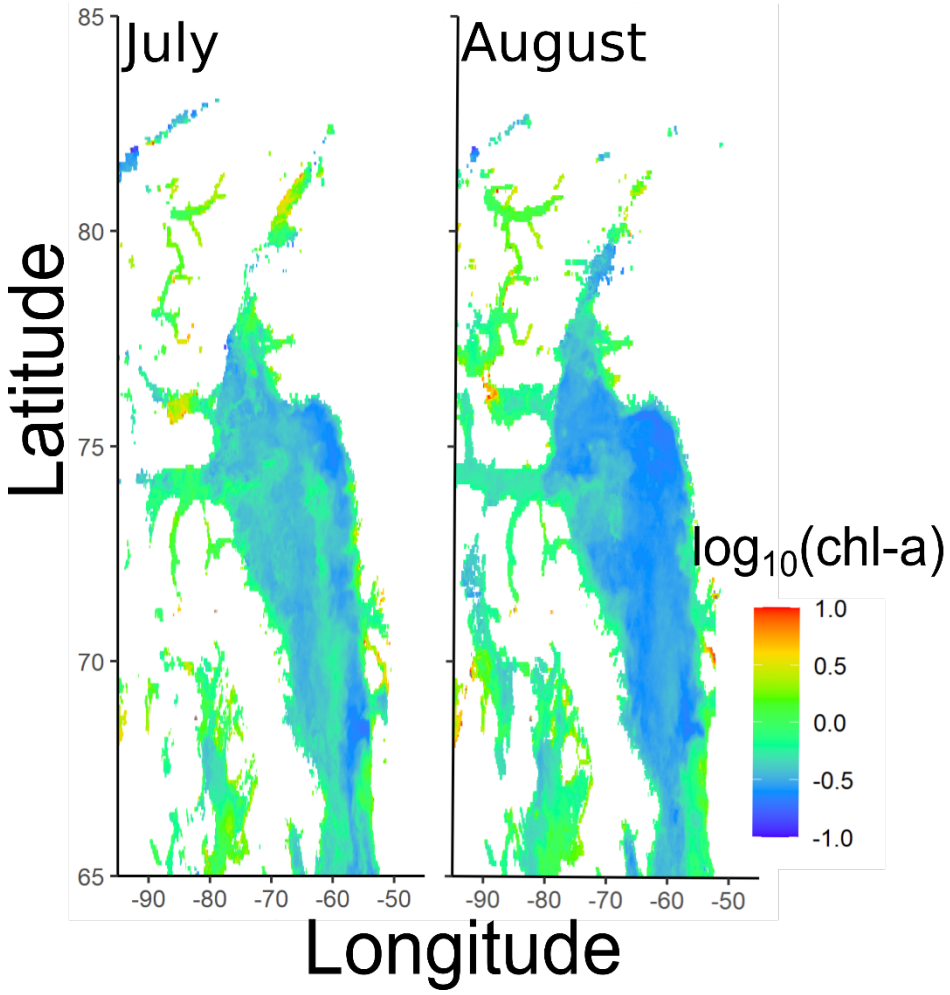

Figure S4: Chlorophyll-a in the study region via satellite observations